

Distribution of higher order spacing ratios in one- plus two-body random matrix ensembles with spin symmetry

Distribution of higher order spacing ratios in embedded ensembles

Priyanka Rao¹, Manan Vyas², and Narendrasinh D. Chavda^{1,a}

¹ Department of Applied Physics, Faculty of Technology and Engineering,
The Maharaja Sayajirao University of Baroda, Vadodara-390001, India

² Instituto de Ciencias Físicas, Universidad Nacional Autónoma de México,
62210 Cuernavaca, Mexico

Received 30 June 2020 / Accepted 28 August 2020

Published online 23 October 2020

Abstract. Random matrix ensembles defined by a mean-field one-body and chaos generating two-body interaction are proved to describe statistical properties of complex interacting many-body quantum systems in general and complex atomic nuclei (or nuclei in the chaotic region) in particular. These ensembles are generically called embedded ensembles of $(1 + 2)$ -body interactions or simply $EE(1 + 2)$ and their GOE random matrix version is called $EGOE(1 + 2)$. In this paper, we study the distribution of non-overlapping spacing ratios of higher-orders in $EGOE(1 + 2)$ for both fermion and boson systems including spin degree of freedom (also without spin) that have their origin in nuclear shell model and the interacting boson model [V.K.B. Kota, N.D. Chavda, *Int. J. Mod. Phys. E* **27**, 1830001 (2018)]. We obtain a very good correspondence between the numerical results and a recently proposed generalized Wigner surmise like scaling relation. These results confirm that the proposed scaling relation is universal in understanding spacing ratios in complex many-body quantum systems. Using spin ensembles, we demonstrate that the higher order spacing ratio distributions can also reveal quantitative information about the underlying symmetry structure (examples are isospin in lighter nuclei and scissors states in heavy nuclei).

1 Introduction

The study of spectral fluctuations is very crucial for understanding the inherent complexities of complex quantum systems. The spectral fluctuation measures, used in many different fields, are modeled through Random Matrix Theory (RMT) [1–3]. These are useful in characterizing distinct phases observed in physical systems such as localized or delocalized phase [4], insulating or metallic phase of many-body systems

^a e-mail: ndchavda-apphy@msubaroda.ac.in

[5,6], integrable or chaotic limit of the underlying classical system [7], and low-lying shell model or mixing regime of nuclear spectra [8,9]. It is now well established that a quantum system is chaotic if its spectral properties follow one of the three classical ensembles, the Gaussian orthogonal (GOE), unitary (GUE) or symplectic (GSE) ensemble depending on the symmetries of the Hamiltonian [10].

The nearest neighbor spacing distribution (NNSD), $P(s)$, giving degree of level repulsion is one of the most popular measures in the study of spectral fluctuations. For time reversal and rotational invariant systems (represented by GOE), as conjectured by Bohigas et al. [11] and proved for certain systems by Haake et al. [12], if a quantum system is chaotic, NNSD follows the Wigner surmise, $P(s) = (\pi/2)s \exp(-\pi s^2/4)$, which indicates the presence of ‘level repulsion’. However, as established by Berry and Tabor [13], if a quantum system is integrable, NNSD follows Poisson distribution, $P(s) = \exp(-s)$, displaying ‘level clustering’.

For a given set of energy levels (or eigenvalues), construction of NNSD requires ‘unfolding’ of the spectra in order to remove the secular variation in the density of eigenvalues [9,10]. This is a cumbersome and non-unique numerical procedure. Also, for many-body systems such as Bose–Hubbard model, unfolding procedure of the spectra becomes non-trivial as the density of states is not a smooth function of energy in the strong interaction domain [14–16]. Similarly, though in the nuclear shell model to a good approximation the density of states is close to an Edgeworth corrected Gaussian, in the interacting boson models of atomic nuclei, the smooth form of the density of states is not determined. Moreover, there are discrepancies between spectral and ensemble unfolding for non-ergodic random matrices [9,17,18].

In the past, Oganessian and Huse [14] introduced the distribution $P(r)$ of the ratio of consecutive level spacings of the energy levels which does not require unfolding as it is independent of the form of the density of the energy levels. Importantly, Atas et al [19] derived expressions for $P(r)$ for the classical GOE, GUE and GSE ensembles of random matrices. The statistics of ratio of spacings has been used to quantify the distance from integrability on finite size lattices [15,16], to investigate many-body localization [14,20–22], to establish that finite many particle quantum systems, modeled by embedded random matrix ensembles, with strong enough interactions follow GOE [23], to study spectral correlations in diffused van der Waals clusters [24] and to analyze spectra of uncorrelated random graph network [25]. Recently, an approximate form for the distribution of spacing ratios for random and localized states in quantum chaotic systems is derived using the 3×3 random matrix model with a possible correction term to it in [26] and a generalized form of Wigner surmise has been proposed for the distribution of non-overlapping spacing ratios of higher-orders [27]. An extension of the Wigner surmise for distribution of higher order spacing ratios was also proposed in the past [28,29] and applied to systems with mixed regular-chaotic dynamics [30].

The Hamiltonian matrix H of a complex quantum system in finite dimensional space contains all information about the system. The nature of the matrix depends on various symmetries imposed on the system. In the presence of symmetries, the Hilbert space of the system splits into invariant subspaces giving block diagonal form for H . Each block is characterized by good quantum numbers corresponding to the respective symmetries. The spectral fluctuations obtained using the discrete levels drawn from the same subspace of the complex quantum systems are known to follow RMT. For mixed spectra, the levels from different blocks are superposed ignoring the symmetries, resulting in level clustering as the actual correlation between the levels is lost. This may give rise to misleading results since the level clustering is also a spectral signature of integrable systems [13]. Recently, in [31] with rigorous numerical evidence, it is shown that the higher order level spacing ratio can also reveal information about symmetry structure of measured or computed levels without desymmetrization, i.e. without symmetry decomposition of the spectra of quantum

systems. With this result, it is also possible to analyze any arbitrary sequence of experimentally observed levels, whose symmetry structure is unknown. This method is straightforward compared to the complicated and approximate methods based on two-level cluster function for a composite spectrum [32,33].

It is important to add that the EGOE(1+2) for fermions with spin degree of freedom correspond to isospin degree of freedom in nuclear shell model [34], for bosons with a fictitious (f) spin degree of freedom correspond to the proton–neutron interacting boson model (or IBM-2) with F -spin [35] and for bosons with spin one degree of freedom correspond to isospin invariant interacting boson model or IBM-3 [36]. For more detailed discussion regarding this correspondence and their significance, see [37–39].

In a large number of investigations carried out during last two decades, it is well established that embedded Gaussian orthogonal ensembles [17,40] of one plus two-body interactions [EGOE(1+2)] apply in a generic way to isolated finite interacting many-particle quantum systems such as nuclei, atoms, quantum dots, small metallic grains, interacting spin systems modeling quantum computing core and so on [37,41–44]. Recently, these models have also been used successfully in understanding high energy physics related problems. Random matrix models with two-body interactions [EGOE(2)] among complex fermions are known as complex Sachdev–Ye–Kitaev models in this area [45–47]. In the present work, we analyze generic properties of non-overlapping higher order spacing ratios for several embedded ensembles, both for fermionic and bosonic systems, with and without spin degree of freedom. We also show that the quantitative information about the symmetry structure of the system can be obtained using higher order spacing ratios for embedded ensembles with spin degree of freedom.

The paper is organized as follows. Analytical results for the probability distribution of the ratio of consecutive level spacings and higher order spacing ratios for GOE are briefly discussed in Section 2. The five different EGOEs, used in the present analysis, are defined in Section 3. Numerical results of the distribution of higher order ratio of consecutive spacings and related averages are presented in Section 4. Finally, Section 5 gives the concluding remarks.

2 Probability distribution of higher order spacing ratios

Understanding and deriving generic results for fluctuation properties has widespread applications in all branches of physics, mathematics, engineering and so on [3,48–52]. Consider an ordered set of eigenvalues (energy levels) e_n , where $n = 1, 2, \dots, d$. The consecutive eigenvalue spacings are given by $s_n = e_{n+1} - e_n$ and the ratios of two nearest neighbor or consecutive eigenvalue spacings are $r_n = s_{n+1}/s_n$. Using an exact calculation for 3×3 Gaussian random matrices, the probability distribution $P(r)$ for consecutive eigenvalue spacings for GOE is derived to be given by [19],

$$P(r) = \frac{27}{8} \frac{(r + r^2)}{(1 + r + r^2)^{5/2}}. \quad (1)$$

Nearest neighbor spacing ratios r probe fluctuations in spectral scales of the order of unit mean spacing. Many different variants of consecutive level spacing ratios have been studied recently [23,26,53]

The non-overlapping higher order spacing ratios can be defined as,

$$r_n^{(k)} = \frac{s_{n+k}^{(k)}}{s_n^{(k)}} = \frac{e_{n+2k} - e_{n+k}}{e_{n+k} - e_n}; \quad n, k = 1, 2, 3 \dots \quad (2)$$

such that there is no shared eigenvalue spacing in the numerator and denominator. Higher order spacing ratios $r^{(k)}$ probe fluctuations in spectral interval of k mean spacings. Recently, it is shown that there exists a scaling relation between the non-overlapping k th order probability distribution $P^k(r)$ and the nearest neighbor spacing ratio distribution $P_\alpha(r)$ with modified parameter α for the class of Wigner–Dyson random matrices [27]. This is verified with numerical evidence from Gaussian and circular ensembles of random matrix theory and for several physical systems such as spin chains, chaotic billiards, Floquet systems and measured nuclear resonances. For GOE, the nearest neighbor spacing ratio distribution $P_\alpha(r)$ is given as,

$$P_\alpha(r) = C_\alpha \frac{(r + r^2)^\alpha}{(1 + r + r^2)^{1+3\alpha/2}}, \quad (3)$$

where C_α is the normalization constant. If the model producing $P^k(r)$ follows RMT, then,

$$\begin{aligned} P^k(r) &= P_\alpha(r), \\ \text{with } \alpha &= \frac{(k+2)(k+1)}{2} - 2, \quad k \geq 1. \end{aligned} \quad (4)$$

The modified parameter $\alpha \geq 4$ can take large integer values and it accounts for the dependence on order k of the spacing ratio. It is also useful to consider $\langle r \rangle = \int r P^k(r) dr$, the average values of spacing ratios r . Similarly, the average values of spacing ratios $\langle r \rangle_\alpha$ can be defined from $P_\alpha(r)$. The values of $\langle r \rangle_\alpha$ corresponding to $k = 2, 3$ and 4 are 1.1747, 1.0855 and 1.0521 respectively. $P^k(r)$, $P_\alpha(r)$ and $\langle r \rangle$ are used in the analysis of energy levels presented in Section 4.

Further, the distribution of higher-order spacing ratios can also be used to understand quantitative information regarding underlying symmetry structure in addition to explaining universal features of fluctuation characteristics. As conjectured by Dyson [54–56] and proved by Gunson [57], the spectral statistics of two superposed circular orthogonal ensemble (COE) spectra converge to that of circular unitary ensemble (CUE). This is expected to be echoed in the distribution of level spacings and spacing ratios as well. Using examples of superposed GOE spectra, billiards, spin-1/2 chains and neutron resonance data, it has been demonstrated that distribution of higher order spacing ratios carry symmetry information [31]. Let us consider an arbitrary sequence of eigenvalues of GOE Hamiltonian H , which is a superposition of \mathbf{m} blocks with each block characterized by good quantum numbers. Then, non-overlapping k th order distribution of spacing ratios, denoted by $P^k(r, \mathbf{m})$ converges to the nearest neighbor spacing ratio distribution $P_\alpha(r)$ [31], in the same way as equation (4),

$$P^k(r, \mathbf{m}) = P_\alpha(r) \quad \text{when } \alpha = k = \mathbf{m}. \quad (5)$$

Note that, here $P^k(r, \mathbf{m} = 1) = P^k(r)$. Therefore, the validity of equation (5) implies that in addition to their fluctuation properties $P^k(r)$ can also reveal the information about the symmetry structure of the composite spectra of complex quantum system.

We analyze $P^k(r)$ for embedded ensembles for fermion and boson systems with and without spin degree of freedom and show that the functional form of $P^k(r)$ is generically identical to $P_\alpha(r)$ for complex many-body quantum systems. Let us add that we are using the ensembles without spin for testing the applicability of equation (4) for quantum many particle systems with interactions. On the other hand, the results for the EE with spin degree of freedom using equation (5) have

direct applications in the analysis of nuclear energy levels giving information about isospin and F -spin; see the discussion at the end of Section 1 and also Section 4 ahead.

3 Embedded ensembles for fermion and boson systems with and without spin degree of freedom

In this section, we define the models that we use to represent complex many-body interacting quantum systems and they are introduced first in nuclear physics in the context of nuclear shell model [9,17,37,40,44]. Embedded Gaussian Orthogonal Ensembles (EGOE) are random matrix models with two-body interactions among its constituents (fermions or bosons) that model Hamiltonians H of interacting many-body quantum systems [9,17,37,40,44]. Given m ($m > 2$) number of spin-less particles (fermions or bosons), they are distributed among N number of single particle (sp) states. As the particles are in an average field generated by other particles, it is appropriate to add a mean-field term $h(1)$ to the Hamiltonian. Thus, with random two-body interactions $V(2)$, the model Hamiltonian is defined by,

$$H = h(1) + \lambda\{V(2)\}. \quad (6)$$

Here, the parameter λ is the strength of the two-body interactions in the units of the average spacing Δ of the sp states and notation $\{ \}$ denotes an ensemble. The $V(2)$ matrix is chosen to be a GOE in two-particle spaces. The one-body Hamiltonian $h(1) = \sum_i \epsilon_i n_i$ is defined by sp energies ϵ_i and n_i are number operators acting on sp states $i = 1, 2, \dots, N$. Distributing these m particles in N sp levels generates the d -dimensional many-particle basis. Action of Hamiltonian H on these many-particle basis states generates EGOE(1+2). When we have fermions as constituents, $d = \binom{N}{m}$ and the two-body matrix elements, chosen to be from GOE, are properly antisymmetrized. These models are denoted by EGOE(1+2) for spin-less fermions. When we have bosons as constituents, $d = \binom{N+m-1}{m}$ and two-body matrix elements, chosen to be from GOE, are symmetrized. These models are denoted by BEGOE(1+2).

In order to analyze universal properties of systems with spin degree of freedom, it is important to include spin \mathbf{s} as an additional degree of freedom in these models. In nuclei the spin \mathbf{s} corresponds to isospin of the nucleons. Given m fermions distributed in Ω number of sp orbitals each with spin $\mathbf{s} = 1/2$, the number of sp states is $N = 2\Omega$. As two-particle spin \mathbf{s} can take two values (0 and 1), $V(2) = V^{s=0}(2) \oplus V^{s=1}(2)$, that is, $V(2)$ is a direct-sum matrix of matrices in spin $s = 0$ and $s = 1$ spaces, chosen to be independent GOEs, with respective dimensions $\Omega(\Omega + 1)/2$ and $\Omega(\Omega - 1)/2$. The many-particle spin S can take values $m/2, m/2 - 1, \dots, 0$ or $1/2$. Thus, EGOE(1+2)- \mathbf{s} is defined by the Hamiltonian $H = h(1) + \lambda_0\{V^{s=0}(2)\} + \lambda_1\{V^{s=1}(2)\}$ [58,59]. The many-particle Hamiltonian matrices are first constructed in smallest spin projection basis (M_S^{min}) using spin-less formulation and then the states with a given S value are projected using the S^2 operator. Many-particle Hamiltonian matrices have a block diagonal structure with each block corresponding to an embedded ensemble with a given total spin S . Similarly, for two species boson systems (as in the proton-neutron interacting boson model of nuclei), it is possible to consider bosons with a fictitious spin ($\mathbf{f} = 1/2$) degree of freedom. Then, we have BEGOE(1+2)- F defined by Hamiltonian $H = h(1) + \lambda_0\{V^{f=0}(2)\} + \lambda_1\{V^{f=1}(2)\}$ [62,63]. Here, $V^{f=0}(2)$ and $V^{f=1}(2)$ are chosen to be independent GOEs in two particle spaces, with respective dimensions $\Omega(\Omega - 1)/2$ and $\Omega(\Omega + 1)/2$. The many-particle spin $F = m/2, m/2 - 1, \dots, 0$ or $1/2$.

Usually, one associates integer spins with bosonic systems and therefore, we have also analyzed boson systems with spin-one degree of freedom, denoted by BEGOE(1+2)-S1 [64]. In the IBM-3 model that applies to medium mass nuclei (no. of protons \sim no. of neutrons), the spin one is isospin $T = 1$ degree of freedom of the bosons in this model [35,36]. Consider m bosons distributed in Ω orbitals each with spin 1. Here, $N = 3\Omega$ and the random interaction $V(2)$ will be of the form $V(2) = V^{s=0}(2) \oplus V^{s=1}(2) \oplus V^{s=2}(2)$ as the two-particle spins are $s = 0, 1$ and 2. Here, $V^{s=0}(2)$, $V^{s=1}(2)$ and $V^{s=2}(2)$ are chosen to be independent GOEs in two-particle spaces with dimensions $\Omega(\Omega + 1)/2$, $\Omega(\Omega - 1)/2$ and $\Omega(\Omega + 1)/2$ respectively. Thus, BEGOE(1+2)-S1 is defined by Hamiltonian $H = h(1) + \lambda_0\{V^{s=0}(2)\} + \lambda_1\{V^{s=1}(2)\} + \lambda_2\{V^{s=2}(2)\}$. The many-particle spin $S = m, m - 1, m - 2, \dots, 0$. In all the five ensembles, without loss of generality, the average spacing between the sp levels is chosen to be unity so that all λ s are unit-less.

In the present work, we make the following choices to analyze spacing ratios:

1. EGOE(1+2) with $m = 6$ and $N = 12$ resulting in H matrix dimension $d = 924$. The sp energies are chosen as $\epsilon_i = i + 1/i$, $i = 1, 2, \dots, 12$ and the interaction strength $\lambda = 0.1$; see reference [41] for details.
2. EGOE(1+2)-s with $m = 6$, $\Omega = 8$, $S = 0 - 3$ with H matrix dimensions 1176, 1512, 420 and 28 respectively. The sp energies are chosen as $\epsilon_i = i + 1/i$, $i = 1, 2, \dots, 8$ and the interaction strength $\lambda = \lambda_0 = \lambda_1 = 0.1$; see references [58,59] for details.
3. BEGOE(1+2) with $m = 10$ and $N = 5$ resulting in H matrix dimension $d = 1001$. The sp energies are chosen as $\epsilon_i = i + 1/i$, $i = 1, 2, \dots, 5$ and the interaction strength $\lambda = 0.03$; see references [60,61] for details.
4. BEGOE(1+2)-F with $m = 10$, $\Omega = 4$, and $F = 0-5$ with H matrix dimensions 196, 540, 750, 770, 594 and 286 respectively. The sp energies are chosen as $\epsilon_i = i + 1/i$, $i = 1, 2, 3, 4$ and the interaction strength $\lambda = \lambda_0 = \lambda_1 = 0.05$; see references [62,63] for details.
5. BEGOE(1+2)-S1 with $m = 8$, $\Omega = 4$, $S = 0-8$ with H matrix dimensions 714, 1260, 2100, 1855, 1841, 1144, 840, 315 and 165 respectively. The sp energies are chosen as $\epsilon_i = i + 1/i$, $i = 1, 2, 3, 4$ and the interaction strength $\lambda = \lambda_0 = \lambda_1 = \lambda_2 = 0.2$; see reference [64] for details.

In all the cases, an ensemble of 500 members each was used. It is important to note that, the value of interaction strength, λ , in all five examples is chosen such that the level fluctuations are GOE type as the focus in the present work is mainly on level fluctuations. With $\lambda = 0.1$, fermion systems are always in Gaussian domain, i.e. eigenvalue density is Gaussian, local density of states is Gaussian and level fluctuations are GOE type, both for EGOE(1+2) [41] and EGOE(1+2)-s [58,59]. For spin-less boson BEGOE(1+2) example, $\lambda = 0.03$ is sufficiently large so that the level fluctuations are GOE [60,61]. Similarly, for boson ensembles with spin degree examples, BEGOE(1+2)-F with $\lambda = 0.05$ [62,63] and BEGOE(1+2)-S1 with $\lambda = 0.2$ [64], again the systems exhibit GOE level fluctuations. Now, we will present numerical results.

4 Numerical results

Using the definition given in Section 2, we have constructed k th order spacing ratio distribution $P^k(r)$ for the EGOE(1+2) models defined in Section 3. We construct

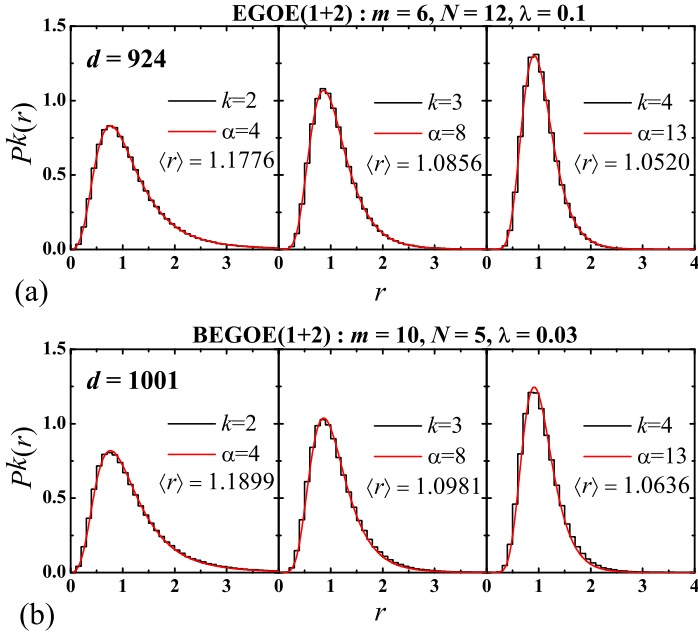


Fig. 1. Histograms represent probability distribution of the k th order spacing ratios r (represented by $P^k(r)$) for a 500 member (a) EGOE(1 + 2) ensemble and (b) BEGOE(1 + 2) ensemble with $k = 2, 3$, and 4. The red smooth curves (represented by $P_\alpha(r)$) are obtained using equation (3) with α values as mentioned in each panel.

numerical histograms for $P^k(r)$ with a bin-size of 0.1 and $k = 2, 3$ and 4 using middle 80% of the spectrum. Figure 1 shows the spacing ratio distribution $P^k(r)$ (black histogram) for embedded ensembles for fermion and boson without spin, EGOE(1 + 2) and BEGOE(1 + 2) respectively. The average values of spacing ratios, $\langle r \rangle$, are also shown in the figure. The ensemble averaged $P^k(r)$ results are compared with $P_\alpha(r)$ (smooth red curves) given by equation (3). Here, the α values are 4, 8 and 13 for $k = 2, 3$ and 4 respectively. Similarly, Figure 2 shows variation in $P^k(r)$ compared with $P_\alpha(r)$ for embedded ensembles with spin degree of freedom, EGOE(1 + 2)-s, BEGOE(1 + 2)- F and BEGOE(1 + 2)- $S1$. For all the examples of embedded ensembles (EE), we find that $\langle r \rangle_{EE} \sim \langle r \rangle_\alpha$. We also obtain good agreement when we include all the levels in the analysis, unlike for nearest neighbor spacing distribution which also gets affected by the choice of unfolding function. As seen from these figures, we obtain excellent agreement between numerical histograms and $P_\alpha(r)$ establishing that equation (4) explains the universal features in variation of higher order spacing ratios in many-body interacting quantum systems, with and without spin degree of freedom.

It is shown that the energy levels of EGOE(1 + 2) close to the ground state (tails of the energy spectrum) generate large fluctuations compared to that of GOE fluctuations by examining NNSD [65] and also $P(r)$ [23]. Going further, it is interesting to test the validity of equation (4) close to the ground state. We analyzed spacing ratio distributions $P^k(r)$ using the lowest 20 energy levels for EGOE(1 + 2) and BEGOE(1 + 2) ensembles with the choice of parameters as outlined in Section 3. The numerical histograms for these are compared with $P_\alpha(r)$ (smooth red curves) in Figure 3. The results show a clear deviation between embedded ensemble $P^k(r)$ and $P_\alpha(r)$ from the trend predicted by equation (4) and deviations increasing with increasing k . Also, $\langle r \rangle_{EE}$ values are found to be smaller than the corresponding $\langle r \rangle_\alpha$

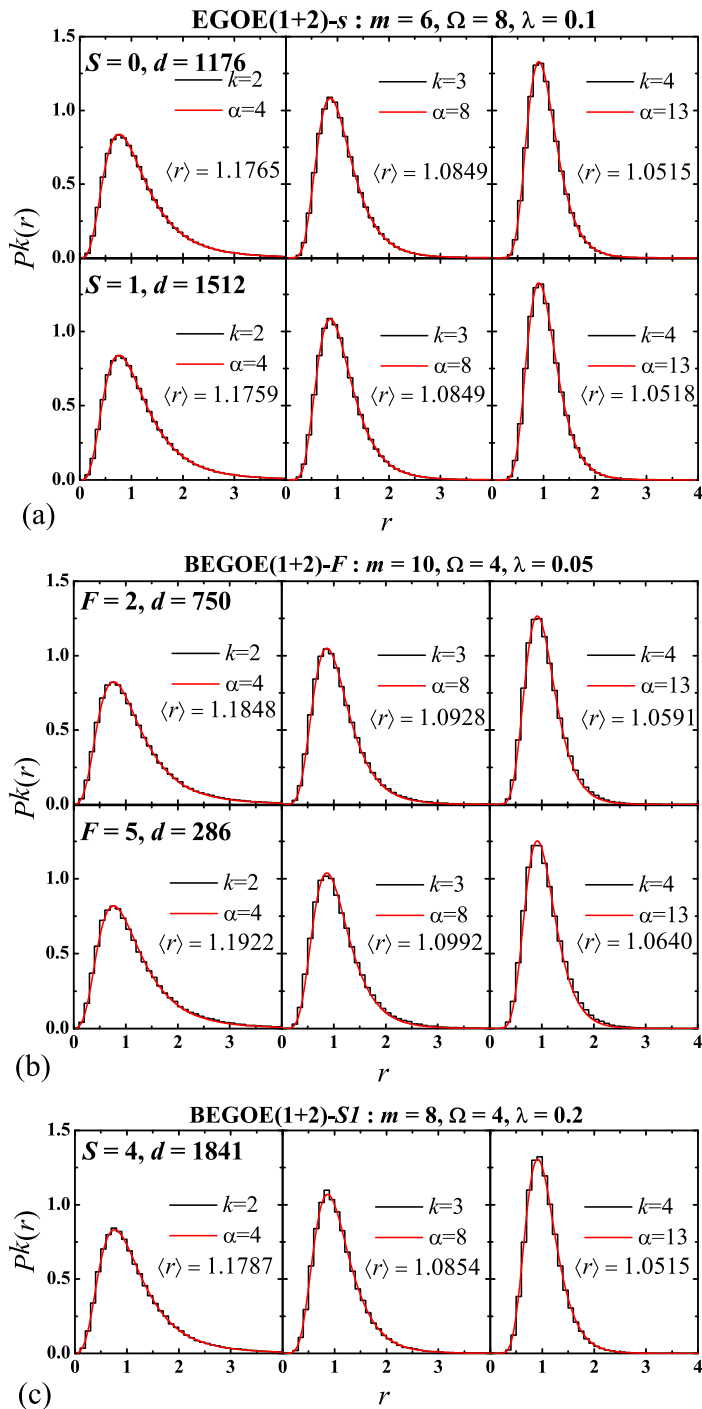


Fig. 2. Same as Figure 1 but results are for a 500-member (a) EGOE(1 + 2)-s (b) BEGOE(1 + 2)-F and (c) BEGOE(1 + 2)-SI. See text for details.

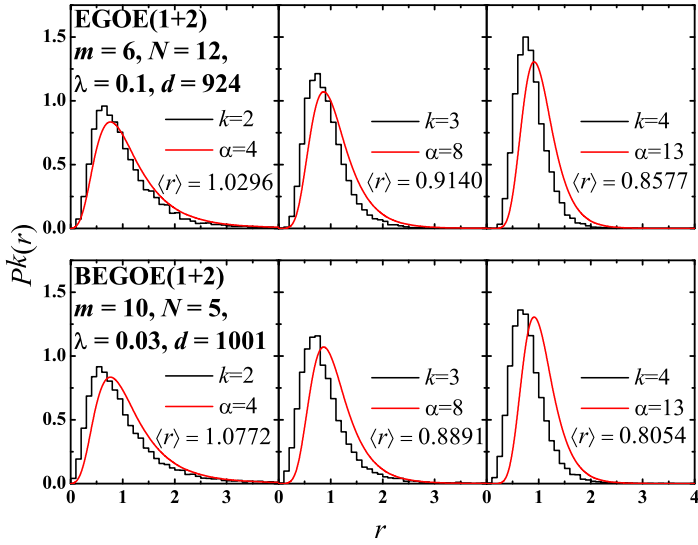


Fig. 3. Probability distribution $P^k(r)$ (histograms) of the k th order spacing ratios r for the lowest 20 energy levels using EGOE(1 + 2) (top panel) and BEGOE(1 + 2) (bottom panel) ensembles. The red smooth curves are obtained using equation (3) with α values as mentioned in each panel.

values. Therefore, although one need not exclude the spectrum tails while analyzing non-overlapping spacing ratios, equation (4) does not explain the variation in spacing ratios close to the ground state.

As pointed out in Section 3, the EGOE(1 + 2) models with spin, EGOE(1 + 2)-s, BEGOE(1 + 2)- F and BEGOE(1 + 2)- $S1$, have specific spin structure: for EGOE(1 + 2)-s and BEGOE(1 + 2)- F , the random interaction matrix $V(2)$ in two-particle spaces is a direct sum of matrices in spin 0 and 1 channels; and for BEGOE(1 + 2)- $S1$, the $V(2)$ matrix in two-particle spaces is a direct sum of matrices in spin 0, 1 and 2 channels. The many-particle Hamiltonian matrix is a block diagonal matrix with each block corresponding to EGOE(1 + 2) with a given spin S . In order to investigate whether $P^k(r)$ carries signatures of these spin structures, we superpose \mathbf{m} independent spin blocks and compare non-overlapping k th order spacing ratio distribution $P^k(r, \mathbf{m})$ with $P_\alpha(r)$ given by equation (3).

For the choice of parameters outlined in Section 3, results are presented in Figures 4–6 respectively for EGOE(1 + 2)-s, BEGOE(1 + 2)- F and BEGOE(1 + 2)- $S1$ examples. In these figures, the ensemble averaged histograms for $P^k(r, \mathbf{m})$ are obtained by arranging the spectra of \mathbf{m} spin blocks in ascending order for each member of the ensemble. Then, ensemble average is computed and plotted as a histogram with bin-size of 0.1 for all k values. The results in the upper panel of Figure 4 are for $P^k(r, \mathbf{m})$ with $\mathbf{m} = 2$ obtained by superposing spectra corresponding to $S = 0$ and $S = 1$ while that in the lower panel are with $\mathbf{m} = 3$ obtained by superposing spectra corresponding to $S = 0$, $S = 1$ and $S = 2$. The smooth red curves are for $P_\alpha(r)$ obtained using equation (3) with α values shown in each panel. A very good agreement between ensemble averaged $P^k(r, \mathbf{m})$ results and $P_\alpha(r)$ is found for with $\alpha = k = \mathbf{m}$ implying that the condition given by equation (5) satisfy. There are clear deviations for all other values. These confirm the presence of \mathbf{m} symmetries. Similarly, results in Figures 5 and 6 also show excellent agreements between ensemble averaged k th order spacing ratio distribution and nearest neighbor spacing ratio results given by equation (3) with $\alpha = k = \mathbf{m}$ confirming the presence of \mathbf{m} symmetries.

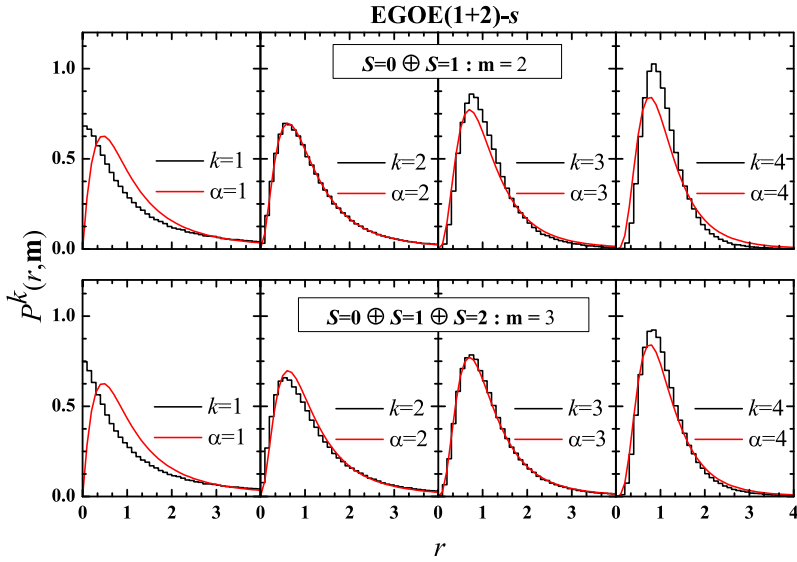


Fig. 4. Histograms represent probability distribution of non-overlapping k th order spacing ratios r of \mathbf{m} independent superposed spin blocks (represented by $P^k(r, \mathbf{m})$) for a 500 member EGOE(1 + 2)-s ensemble. Upper panel shows results for $\mathbf{m} = 2$, with spins $S = 0-1$, while lower panel shows results for $\mathbf{m} = 3$, with spins $S = 0-2$. The histograms are compared with the red smooth curves obtained using equation (3) with α values as mentioned in each panel.

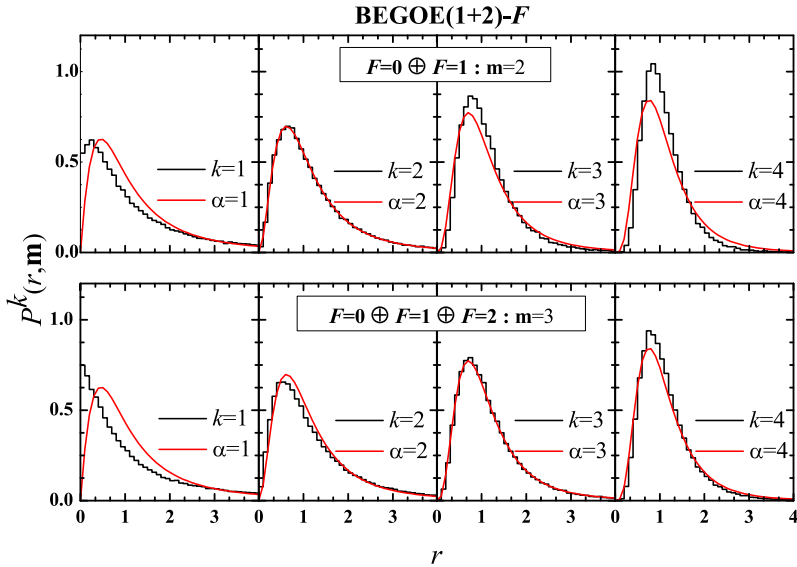


Fig. 5. Same as Figure 4 but results are for \mathbf{m} superposed spectra of a 500-member BEGOE(1 + 2)- F ensemble. Upper panel shows results for $\mathbf{m} = 2$ with spins $F = 0-1$ while lower panel shows results for $\mathbf{m} = 3$ with spins $F = 0-2$. See Figure 4 for details.

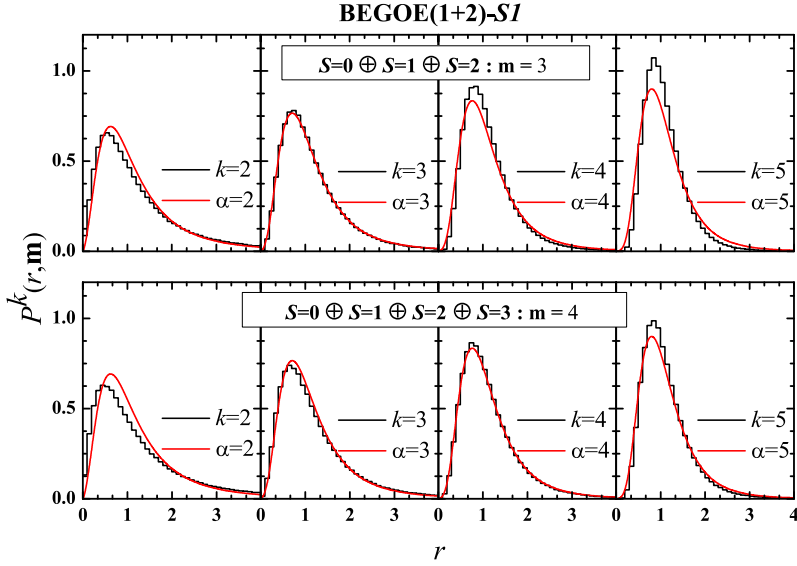


Fig. 6. Same as Figure 4 but results are for \mathbf{m} superposed spectra of a 500 member BEGOE(1+2)-S1 ensemble. Upper panel shows results for $\mathbf{m} = 3$ with spins $S = 0-2$ while lower panel shows results for $\mathbf{m} = 4$ with spins $S = 0-3$. See Figure 4 for details.

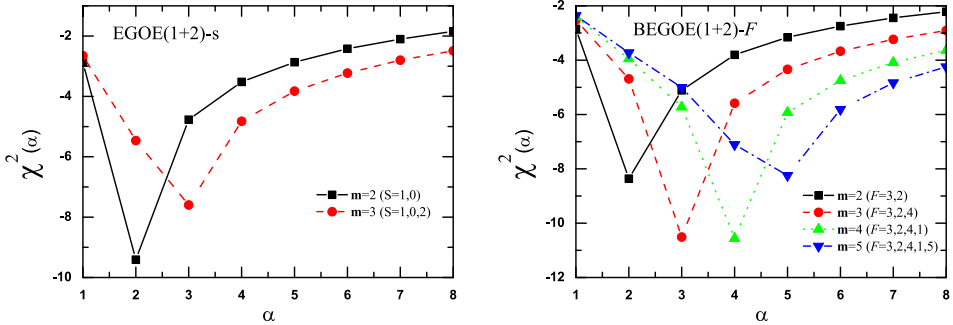


Fig. 7. Variation in $\chi^2(\alpha)$ vs. α for EGOE(1+2)-s ensemble (left panel) and BEGOE(1+2)-F ensemble (right panel) for different \mathbf{m} values as mentioned in the panel. The minimum values of $\chi^2(\alpha)$ indicates $P^k(r, \mathbf{m}) \sim P_\alpha(r)$ for \mathbf{m} superposed spectra.

In order to obtain the best quantitative estimate for α , we calculate χ^2 measure defined as,

$$\chi^2(\alpha) = \log \left\{ \int_0^\infty dr (P^k(r, \mathbf{m}) - P_\alpha(r))^2 \right\}. \quad (7)$$

Here, minimum value of $\chi^2(\alpha)$ implies $P^k(r, \mathbf{m}) \sim P_\alpha(r)$. Figure 7 shows the variation in $\chi^2(\alpha)$ as a function of α for various \mathbf{m} values. The left panel gives the results for EGOE(1+2)-s and the right panel gives the results for BEGOE(1+2)-F. We have not included spectra of maximum spin $S = S_{max}$ for EGOE(1+2)-s and spectra of minimum spin $F = F_{min}$ for BEGOE(1+2)-F due to small matrix dimensions. The minimum value for $\chi^2(\alpha)$ is obtained at $\alpha = k = \mathbf{m}$, which is in agreement with the results shown in Figures 4 and 5. We have also confirmed this result with

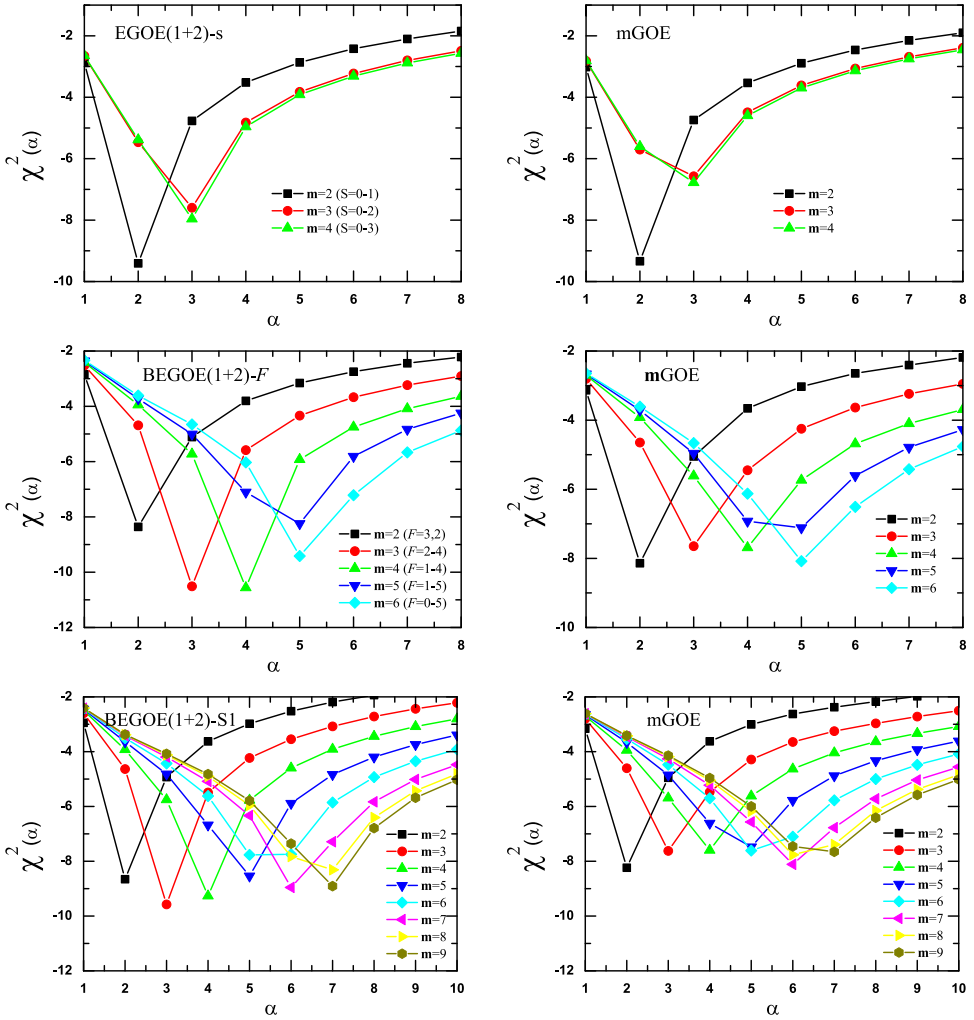


Fig. 8. Variation in $\chi^2(\alpha)$ vs. α for EGOE(1 + 2)-s (top left panel), BEGOE(1 + 2)- F (middle left panel) and BEGOE(1 + 2)-S1 (bottom left panel) for different \mathbf{m} values as indicated in the panel. Right panel represents variation in $\chi^2(\alpha)$ vs. α for superposed \mathbf{m} GOE spectra of exactly same dimensions corresponding to results in the left panel for EGOE(1 + 2)-s, BEGOE(1 + 2)- F and BEGOE(1 + 2)-S1 respectively. See text for further details.

other combinations of superposed spectra corresponding to different spin sectors. It is important to note that similar results were obtained by combining \mathbf{m} blocks of EGOE and GOE spectra. Therefore, the distribution of higher order level spacing ratios are independent of the state density of the spectra and can also be useful in extracting symmetry information of the composite spectra.

There are deviations from obtaining minimum for $\chi^2(\alpha)$ at $\alpha = k = \mathbf{m}$ when the dimension of a given spin block is very small. Figure 8 shows variation in $\chi^2(\alpha)$ as a function of α for EGOE(1 + 2)-s (top left panel), BEGOE(1 + 2)- F (middle left panel) and BEGOE(1 + 2)-S1 (bottom left panel). Results are shown for various \mathbf{m} values. For EGOE (1 + 2)-s, the minimum for $\chi^2(\alpha)$ is not at $\alpha = k = \mathbf{m}$ for $\mathbf{m} = 4$ as it is obtained by superposing four spin blocks corresponding to $S = 0-3$. Here, $S = 3$ is the

maximum allowed spin and has the smallest dimension (28 compared to dimensions 1176, 1512, 420 respectively for spins $S = 0$, $S = 1$ and $S = 2$). Similarly, deviations are seen in minimum for $\chi^2(\alpha)$ from $\alpha = k = \mathbf{m}$ at $\mathbf{m} = 6$ for BEGOE(1+2)- F and for $\mathbf{m} = 6-9$ for BEGOE(1+2)- $S1$. Going further, we superposed \mathbf{mGOE} spectra of exact same dimensions (see Fig. 8) corresponding to EGOE(1+2)- s (top right panel), BEGOE(1+2)- F (middle right panel) and BEGOE(1+2)- $S1$ (bottom right panel). These results also show similar deviations in minimum for $\chi^2(\alpha)$ confirming that there are finite-size effects.

Turning to the important question of applications, a re-examination of nuclear data for energy levels in nuclei using the results of higher order spacing ratios reported here is expected to give new information about symmetries in nuclei. For example: (i) in ^{26}Al and ^{30}P energy levels up to ~ 8 MeV excitation with isospin $T = 0$ and $T = 1$ are available [66,67] and they can be analyzed using EGOE(1+2)- s with spin being isospin; (ii) scissors levels in 2.5–4 MeV excitation in heavy deformed nuclei with the low-lying levels having $F = N/2$ and scissors levels $F = N/2 - 1$ [68] and they can be analyzed using BEGOE(1+2)- F ; (iii) excited 2^+ and 4^+ levels in nuclei across the periodic table with various symmetries of IBM and its extensions [69–73]. In addition, analyzing energy levels from large shell model and also IBM-2 and IBM-3 models for higher order spacing ratios may give new information about symmetries in nuclei. These studies are for future. In the past NNSD but not higher order spacings are used in the analysis of all the data listed above [37].

5 Conclusion

We have analyzed higher order level spacing ratios for interacting many-body quantum systems with and without spin degree of freedom. Complex many-body systems such as atomic nuclei are modeled by EGOE(1+2) for fermionic and bosonic systems with and without spin degree of freedom. We have obtained excellent agreement between numerical results for higher order spacing ratios and Wigner surmise like scaling relation. Thus, this scaling relation is universal to understand higher order spacing ratios in complex many-body quantum systems (fermionic as well as bosonic) with rotational and time-reversal invariance, with and without spin degree of freedom. We have shown that the higher order spacing ratio distributions can also reveal quantitative information about underlying symmetry structure. Hence, the analysis of higher order spacing ratios is not only useful in studying spectral fluctuations but also reveals quantitative information about symmetry structure of complex quantum systems. As briefly mentioned at the end of the previous section, there is good amount of nuclear structure data that can be analyzed to give new information about symmetries such as isospin symmetry and F -spin symmetry but the data analysis is postponed to a future publication. Although not shown explicitly, these results are expected to extend to the unitary versions EGUE(1+2) (for both fermionic and bosonic systems, with and without spin degree of freedom) as well. It would be interesting to analyze complex spacing ratios [74] to characterize integrable and chaotic dynamics for the embedded unitary ensembles with various symmetries like spin, parity, total angular momentum etc. [37,44] and characterize universality of transition to chaos [75].

Authors thank V.K.B. Kota for many useful discussions. P.R. and N.D.C. acknowledge support from Department of Science and Technology (DST), Government of India [Project No.: EMR/2016/001327]. M.V. acknowledges financial support from UNAM/DGAPA/PAPIIT research grant IA101719.

Author contribution statement

All authors contributed equally and agreed to the published version of the manuscript.

Publisher's Note The EPJ Publishers remain neutral with regard to jurisdictional claims in published maps and institutional affiliations.

References

1. C.E. Porter, *Statistical theories of spectra: fluctuations* (Academic Press, New York, 1965)
2. M.L. Mehta, *Random matrices* (Elsevier B.V., Netherlands, 2004)
3. G. Akemann, J. Baik, P. Di Francesco (Eds.), *The Oxford handbook of random matrix theory* (Oxford University Press, New York, 2011)
4. S.D. Geraedts, R. Nandkishore, N. Regnault, Phys. Rev. B **93**, 174202 (2016)
5. H. Hasegawa, Y. Sakamoto, Prog. Theor. Phys. Suppl. **139**, 112 (2000)
6. S.M. Nishigaki, Phys. Rev. E **59**, 2853 (1999)
7. L. Reichl, *The transition to chaos: conservative classical systems and quantum manifestations* (Springer Science and Business Media, 2013)
8. H.A. Weidenmüller, G.E. Mitchell, Rev. Mod. Phys. **81**, 539 (2009)
9. T.A. Brody, J. Flores, J.B. French, P.A. Mello, A. Pandey, S.S. Wong, Rev. Mod. Phys. **53**, 385 (1981)
10. F. Haake, *Quantum signatures of chaos* (Springer-Verlag, Heidelberg, 2010)
11. O. Bohigas, M.-J. Giannoni, C. Schmit, Phys. Rev. Lett. **52**, 1 (1984)
12. S. Heusler, S. Müller, A. Altland, P. Braun, F. Haake, Phys. Rev. Lett. **98**, 044103 (2007)
13. M.V. Berry, M. Tabor, Proc. Roy. Soc. (London) **A356**, 375 (1977)
14. V. Oganesyan, D.A. Huse, Phys. Rev. B **75**, 155111 (2007)
15. C. Kollath, G. Roux, G. Biroli, A.M. Läuchli, J. Stat. Mech. **2010**, P08011 (2010)
16. M. Collura, H. Aufderheide, G. Roux, D. Karevski, Phys. Rev. A **86**, 013615 (2012)
17. O. Bohigas, J. Flores, Phys. Lett. B **34**, 261 (1971)
18. R.J. Leclair, R.U. Haq, V.K.B. Kota, N.D. Chavda, Phys. Lett. A **372**, 4373 (2008)
19. Y.Y. Atas, E. Bogomolny, O. Giraud, G. Roux, Phys. Rev. Lett. **110**, 084101 (2013)
20. V. Oganesyan, A. Pal, D.A. Huse, Phys. Rev. B **80**, 115104 (2009)
21. A. Pal, D.A. Huse, Phys. Rev. B **82**, 174411 (2010)
22. S. Iyer, V. Oganesyan, G. Refael, D.A. Huse, Phys. Rev. B **87**, 134202 (2013)
23. N.D. Chavda, V.K.B. Kota, Phys. Lett. A **377**, 3009 (2013)
24. S.K. Haldar, B. Chakrabarti, N.D. Chavda, T.K. Das, S. Canuto, V.K.B. Kota, Phys. Rev. A **89**, 043607 (2014)
25. G. Torres-Vargas, R. Fossion, J.A. Méndez-Bermúdez, Physica A **2019**, 123298 (2019)
26. S. Harshini Tekur, S. Kumar, M.S. Santhanam, Phys. Rev. E **97**, 062212 (2018)
27. S. Harshini Tekur, Udaysinh T. Bhosale, M.S. Santhanam, Phys. Rev. B **98**, 104305 (2018)
28. P.B. Kahn, C.E. Porter, Nucl. Phys. **48**, 385 (1963)
29. A.Y. Abul-Magd, M.H. Simbel, Phys. Rev. E **60**, 5371 (1999)
30. A.Y. Abul-Magd, M.H. Simbel, Phys. Rev. E **62**, 4792 (2000)
31. S. Harshini Tekur, M.S. Santhanam, [arXiv:1808.08541](https://arxiv.org/abs/1808.08541)
32. T. Guhr, H.A. Weidenmüller, Chem. Phys. **146**, 21 (1990)
33. L. Leviandier, M. Lombardi, R. Jost, J.P. Pique, Phys. Rev. Lett. **56**, 2449 (1986)
34. P.J. Brussaard, P.W.M. Glaudemans, *Shell model applications in nuclear spectroscopy* (North Holland, Amsterdam, 1977)
35. F. Iachello, A. Arima, *The interacting boson model* (Cambridge University Press, Cambridge, 1987)
36. V.K.B. Kota, R. Sahu, *Structure of medium mass nuclei: deformed shell model and spin-isospin interacting boson model* (CRC press, Taylor & Francis group, Boca Raton, FL, 2017)

37. V.K.B. Kota, *Embedded random matrix ensembles in quantum physics* (Springer-Verlag, Heidelberg, 2014)
38. V.K.B. Kota, N.D. Chavda, Int. J. Mod. Phys. E **27**, 1830001 (2018)
39. V.K.B. Kota, N.D. Chavda, Entropy **2018**, 541 (2018)
40. J.B. French, S.S.M. Wong, Phys. Lett. B **33**, 449 (1970)
41. V.K.B. Kota, Phys. Rep. **347**, 223 (2001)
42. H.A. Weidenmüller, G.E. Mitchell, Rev. Mod. Phys. **81**, 539 (2009)
43. J.M.G. Gomez, K. Kar, V.K.B. Kota, R.A. Molina, A. Relaño, J. Retamosa, Phys. Rep. **499**, 103 (2011)
44. M. Vyas, Ph.D. Thesis, M.S. University of Baroda, Vadodara, India, 2011, <https://arxiv.org/abs/1710.08333> (2017)
45. R.A. Davison, W. Fu, A. Georges, Y. Gu, K. Jensen, S. Sachdev, Phys. Rev. B **95**, 155131 (2017)
46. K.J. Bulycheva, J. High Energ. Phys. **12**, 069 (2017)
47. V. Rosenhaus, J. Phys. A **52**, 323001 (2019)
48. R.N. Mantegna, H.E. Stanley, *An introduction to econophysics: correlations and complexity in finance* (Cambridge University Press, UK, 2000)
49. M. Wright, R. Weaver, *New directions in linear acoustics and vibration: quantum chaos, random matrix theory and complexity* (Cambridge University Press, New York, 2010)
50. Z. Bai, J.W. Silverstein, *Spectral analysis of large dimensional random matrices*, 2nd ed. (Springer-Verlag, New York, 2010)
51. P.J. Forrester, *Log-gases and random matrices* (Princeton University Press, USA, 2010)
52. R. Couillet, M. Debbah, *Random matrix methods for wireless communications* (Cambridge University Press, New York, 2011)
53. N.D. Chavda, H.N. Deota, V.K.B. Kota, Phys. Lett. A **378**, 3012 (2014)
54. F.J. Dyson, J. Math. Phys. **3**, 140 (1962)
55. F.J. Dyson, J. Math. Phys. **3**, 157 (1962)
56. F.J. Dyson, J. Math. Phys. **3**, 166 (1962)
57. J. Gunson, J. Math. Phys. **3**, 752 (1962)
58. V.K.B. Kota, N.D. Chavda, R. Sahu, Phys. Lett. A **359**, 381 (2006)
59. M. Vyas, V.K.B. Kota, N.D. Chavda, Phys. Rev. E **81**, 036212 (2010)
60. N.D. Chavda, V. Potbhare, V.K.B. Kota, Phys. Lett. A **311** 331 (2003)
61. N.D. Chavda, V.K.B. Kota, V. Potbhare, Phys. Lett. A **376**, 2972 (2012)
62. N.D. Chavda, V.K.B. Kota, Ann. Phys. (Berlin) **529**, 1600287 (2017)
63. M. Vyas, N.D. Chavda, V.K.B. Kota, V. Potbhare, J. Phys. A: Math. Theor. **45**, 265203 (2012)
64. H.N. Deota, N.D. Chavda, V.K.B. Kota, V. Potbhare, M. Vyas, Phys. Rev. E **88**, 022130 (2013)
65. J. Flores, M. Horoi, M. Müller, T.H. Seligman, Phys. Rev. E **63**, 026204 (2001)
66. G.E. Mitchell, E.G. Bilpuch, P.M. Endt, J.F. Shriner Jr., Phys. Rev. Lett. **61**, 1473 (1988)
67. J.F. Shriner Jr., C.A. Grossmann, G.E. Mitchell, Phys. Rev. C **62**, 054305 (2000)
68. J. Enders, T. Guhr, N. Huxel, P. von Neumann-Cosel, C. Rangacharyulu, A. Richter, Phys. Lett. B **486**, 273 (2000)
69. A.Y. Abul-Magd, H.L. Harney, M.H. Simbel, H.A. Weidenmüller, Ann. Phys. (N.Y.) **321**, 560 (2006)
70. A. Al-Sayed, A.Y. Abul-Magd, Phys. Rev. C **74**, 037301 (2006)
71. M.A. Jafarizadeh, N. Fouladi, H. Sabri, B.R. Maleki, Nucl. Phys. A **890**, 29 (2012)
72. H. Sabri, Nucl. Phys. A **941**, 364 (2015)
73. A. Heusler, R.V. Jolos, T. Faestermann, R. Hertenberg, H.-F. Wirth, P. von Brentano, Phys. Rev. C **93**, 054321 (2016)
74. L. Sá, P. Ribeiro, T. Prosen, Phys. Rev. X **10**, 021019 (2020)
75. A.L. Corps, A. Relaño, Phys. Rev. E **101**, 022222 (2020)



Structure of wavefunction for interacting bosons in mean-field with random k -body interactions

Priyanka Rao, N.D. Chavda*

Department of Applied Physics, Faculty of Technology and Engineering, The Maharaja Sayajirao University of Baroda, Vadodara-390001, India



ARTICLE INFO

Article history:

Received 28 November 2020
 Received in revised form 9 February 2021
 Accepted 13 March 2021
 Available online 19 March 2021
 Communicated by M.G.A. Paris

Keywords:

Interacting bosons
 Dense limit
 Embedded ensembles
 Many-body interactions
 Strength functions
 Number of principal components

ABSTRACT

Wavefunction structure is analyzed for dense interacting many-boson systems using Hamiltonian H , which is a sum of one-body $h(1)$ and an embedded GOE of k -body interaction $V(k)$ with strength λ . In the first analysis, a complete analytical description of the variance of the strength function as a function of λ and k is derived and the marker λ_t defining thermalization region is obtained. In the strong coupling limit ($\lambda > \lambda_t$), the conditional q -normal density describes Gaussian to semi-circle transition in strength functions as body rank k of the interaction increases. In the second analysis, this interpolating form of the strength function is utilized to describe the fidelity decay after k -body interaction quench and also to obtain the smooth form for the number of principal components, a measure of chaos in finite interacting many-particle systems. The smooth form very well describes embedded ensemble results for all k values.

© 2021 Elsevier B.V. All rights reserved.

1. Introduction

It is now well established that Random Matrix Theory, due to its universality [1], successfully describes the spectral as well as wavefunction properties of isolated finite many-particle quantum systems [2]. The spectral statistics deals only with the energy eigenvalues while the statistical properties related to the structure of the wavefunctions can reveal different layers of chaos and hence give profound understanding of various problems in the field of quantum many-body chaos and thermalization, in isolated finite interacting particle systems such as atomic nuclei, atoms, mesoscopic systems (quantum dots, small metallic grains), interacting spin systems modeling quantum computing core, ultra-cold atoms and quantum black holes with SYK model and so on [2–9]. To analyze the wavefunction properties, it is very crucial to examine the so-called strength functions (also known as local density of states) in detail, as they give information about how a particular basis state spreads onto the eigenstates. The chaos measures like number of principal components (NPC), information entropy, fidelity decay etc. can also be determined by examining the general features of the strength functions [2].

The statistical properties of isolated finite many-particle quantum systems investigated by employing random matrix ensembles

are generally referred as Gaussian ensembles (and in particular the Gaussian orthogonal ensemble (GOE)) for m -particle system. They involve interaction up to m -body in character and are dominated by the m -body interactions. However, constituents of isolated quantum systems interact via few-body interactions. Hence the concept of embedded ensemble (EE) of k -body interaction, in particular EGOE(k) (GOE version of EE(k)) was introduced by French and co-workers [10,11]. These models for the particles in a mean-field and interacting via two-body interactions ($k = 2$) and their various extended versions form good models for understanding various aspects of chaos in interacting particle systems [2] and they are investigated in detail both for fermion systems (called EGOE(1+2)) [12–17] as well as boson systems (called BEGOE(1+2) with 'B' for bosons) [18–23]. Here, with m particles distributed in N single particle (sp) states, two limiting situations exist, one is the dilute limit (defined as $m \rightarrow \infty$, $N \rightarrow \infty$ and $m/N \rightarrow 0$) and another is the dense limit (defined by $m \rightarrow \infty$, $N \rightarrow \infty$ and $m/N \rightarrow \infty$). In the dilute limit, one can expect similar behavior for both fermion and boson systems while the dense limit is feasible only for boson systems and therefore the focus was on the dense limit in BEGOE investigations [18–24]. For EGOE(1+2) in dilute limit and for BEGOE(1+2) in dense limit, as a function of the two-body interaction strength λ (measured in units of the average spacing between the one-body mean-field sp levels), exhibits three transition or chaos markers (λ_C , λ_F , λ_t): (a) as the two-body interaction is turned on, level fluctuations exhibit a transition from Poisson to GOE at $\lambda = \lambda_C$; (b) with further increase in λ , the

* Corresponding author.

E-mail address: ndchavda-aphy@msubaroda.ac.in (N.D. Chavda).

strength functions make a transition from Breit-Wigner (BW) form to Gaussian form at $\lambda = \lambda_F > \lambda_C$; and (c) beyond $\lambda = \lambda_F$, there is a region of thermalization around $\lambda = \lambda_t$ where the basis dependent thermodynamic quantities like entropy behave alike. It is important to note that the transitions mentioned above are inferred from large number of numerical calculations and they are well verified to be valid in the bulk part of the spectrum. For further details see [2] and references there in.

Going beyond two-body interaction, it is seen that the higher body interactions i.e. $k > 2$ play an important role in strongly interacting quantum systems [25,26], nuclear physics [27], quantum black holes [7,28] and wormholes [29] with SYK model and also in quantum transport in disordered networks connected by many-body interactions [30–32]. Therefore, it is necessary to extend the analysis of EE to higher k -body interactions in order to understand these problems. From the previous studies, it is known that with EGOE(k) or (BEGOE(k)), the eigenvalue density for a system of m fermions/bosons in N sp states changes from Gaussian form to semi-circle as k changes from 2 to m [2,6,13,33]. Very recently, q -Hermite polynomials have been employed to study spectral densities of the so-called SYK model [34,35] and quantum spin glasses [36], along with studying the strength functions and fidelity decay (also known as survival or return probability) in EE, both for fermion as well as boson systems [33]. The smooth form of eigenvalue density can be given by the so-called q -normal distribution f_{qN} and formulas for parameter q in terms of m , N and k are derived for fermionic and bosonic EE(k) in [33] which explain the Gaussian to semi-circle transition in spectral densities, strength functions and fidelity decay in many-body quantum systems as a function of rank k of interactions. Recently, the lower-order bivariate reduced moments of the transition strengths are examined for the action of a transition operator on the eigenstates generated by EGOE(k) and it is shown that the ensemble averaged distribution of transition strengths follows a bivariate q -normal distribution f_{biv-qN} and a formula for NPC in the transition strengths from a state is obtained [37]. Very recently, analytical formulas for the lowest four moments of the strength functions for fermion systems modeled by EGOE($1+k$) are derived and it is shown that the conditional q -normal density f_{CqN} can be used to represent strength functions in the strong coupling limit [38]. One can expect similar behavior for isolated finite interacting boson systems with k -body interactions in the dense limit. The purpose of the present letter is firstly to demonstrate that in strong coupling domain (in the thermalization region), the strength functions indeed can be represented by the conditional q -normal distribution f_{CqN} in the dense interacting boson systems interacting via k -body interaction. Secondly, using f_{CqN} form and parameters that enter in this form, fidelity decay is described in BEGOE($1+k$) and an analytical formula for NPC is derived.

The Letter is organized as follows. We briefly introduce BEGOE($1+k$) and q -Hermite polynomials along with their generating function and conditional q -normal distribution in Section 2. The numerical results of the variation of parameter q as a function of k -body interaction strength λ in BEGOE($1+k$) are presented in Section 3. Also the formula of q for BEGOE(k) is given for the sake of completeness, even though it is clearly given in [6,33]. Further, a complete analytical description of the variance of the strength function, in terms of the correlation coefficient ζ , for BEGOE($1+k$) is given and (m , N , k) dependence of marker λ_t is derived. In Section 4, the results for the variation of strength function, in the strong coupling domain ($\lambda \gg \lambda_t$), are presented as a function of body rank k and ensemble averaged results are compared with smooth forms given by f_{CqN} . In Section 5 the interpolating form f_{CqN} for the strength function is utilized to describe the fidelity decay after random k -body interaction quench in BEGOE($1+k$) in the thermalization region. Further, two-parameter (ζ and q) an-

alytical formula for NPC is derived as a function of energy for k -body interaction and tested with numerical embedded ensemble results in Section 6. Finally, the concluding remarks are given in Section 7.

2. Preliminaries

2.1. Embedded bosonic ensembles - BEGOE($1+k$)

Consider m spinless bosons distributed in N degenerate sp states interacting via k -body ($1 \leq k \leq m$) interactions. Distributing these m bosons in all possible ways in N sp states generates many-particle basis of dimension $d = \binom{N+m-1}{m}$. The k -body random Hamiltonian $V(k)$ is defined as,

$$V(k) = \sum_{k_a, k_b} V_{k_a, k_b} B^\dagger(k_a) B(k_b). \quad (1)$$

Here, operators $B^\dagger(k_a)$ and $B(k_b)$ are k -boson creation and annihilation operators. They obey the boson commutation relations. V_{k_a, k_b} are the symmetrized matrix elements of $V(k)$ in the k -particle space with the matrix dimension being $d_k = \binom{N+k-1}{k}$. They are chosen to be randomly distributed independent Gaussian variables with zero mean and unit variance, in other words, k -body Hamiltonian is chosen to be a GOE. BEGOE(k) is generated by action of $V(k)$ on the many-particle basis states. Due to k -body nature of interactions, there will be zero matrix elements in the many-particle Hamiltonian matrix, unlike a GOE. By construction, we have a GOE for the case $k = m$. For further details about these ensembles, their extensions and applications, see [2,39,40] and references therein.

In realistic systems, bosons also experience mean-field generated by presence of other bosons in the system and hence, it is more appropriate to model these systems by BEGOE($1+k$) defined by,

$$H = h(1) + \lambda V(k) \quad (2)$$

Here, the one-body operator $h(1) = \sum_{i=1}^N \epsilon_i n_i$ is described by fixed sp energies ϵ_i ; n_i is the number operator for the i th sp state. The parameter λ represents the strength of the k -body interaction and it is measured in units of the average mean spacing of the sp energies defining $h(1)$. In this analysis, we have employed fixed sp energies $\epsilon_i = i + 1/i$ in defining the mean-field Hamiltonian $h(1)$. As the dense limit is more interesting for bosons, for numerical study, we have chosen $N = 5$, $m = 10$ with space dimensionality of $d = 1001$ and varied k from 2 to m . It is now known that in nuclear reactions and strongly interacting quantum systems $k = 2, 3, 4$ are of physical importance [7,25,26]. However for the sake of completeness, to study the generic features of embedded ensembles and the possibility of higher k becoming prominent, we address $k = 2$ to m .

2.2. q -Hermite polynomials and conditional q -normal distribution

The q -Hermite polynomials were first introduced by L. J. Rogers in Mathematics. Consider q numbers $[n]_q$ defined as $[n]_q = (1 - q)^{-1} (1 - q^n)$. Then, $[n]_{q \rightarrow 1} = n$, and $[n]_q! = \prod_{j=1}^n [j]_q$ with $[0]_q! = 1$. Now, q -Hermite polynomials $H_n(x|q)$ are defined by the recursion relation [41],

$$x H_n(x|q) = H_{n+1}(x|q) + [n]_q H_{n-1}(x|q) \quad (3)$$

with $H_0(x|q) = 1$ and $H_{-1}(x|q) = 0$. Note that for $q = 1$, the q -Hermite polynomials reduce to normal Hermite polynomials (related to Gaussian) and for $q = 0$ they will reduce to Chebyshev

polynomials (related to semi-circle). Importantly, q -Hermite polynomials are orthogonal within the limits $\pm 2/\sqrt{1-q}$, with the q -normal distribution $f_{qN}(x|q)$ as the weight function defined by [37],

$$f_{qN}(x|q) = \frac{\sqrt{1-q}}{2\pi\sqrt{4-(1-q)x^2}} \times \prod_{i=0}^{\infty} (1-q^{i+1})[(1+q^i)^2 - (1-q)q^i x^2]. \quad (4)$$

Here, $-2/\sqrt{1-q} \leq x \leq 2/\sqrt{1-q}$ and $q \in [0, 1]$. Note that $\int_{s(q)} f_{qN}(x|q) dx = 1$ over the range $s(q) = (-2/\sqrt{1-q}, 2/\sqrt{1-q})$. It is seen that in the limit $q \rightarrow 1$, $f_{qN}(x|q)$ will take Gaussian form and in the limit $q = 0$ semi-circle form. Now the bivariate q -normal distribution $f_{biv-qN}(x, y|\zeta, q)$ is defined as follows [37,42],

$$f_{biv-qN}(x, y|\zeta, q) = f_{qN}(x|q) f_{CqN}(y|x; \zeta, q) = f_{qN}(y|q) f_{CqN}(x|y; \zeta, q) \quad (5)$$

where ζ is the bivariate correlation coefficient and the conditional q -normal densities, f_{CqN} can be given as,

$$f_{CqN}(x|y; \zeta, q) = f_{qN}(x|q) \prod_{i=0}^{\infty} \frac{(1-\zeta^2 q^i)}{h(x, y|\zeta, q)}; \\ f_{CqN}(y|x; \zeta, q) = f_{qN}(y|q) \prod_{i=0}^{\infty} \frac{(1-\zeta^2 q^i)}{h(x, y|\zeta, q)}; \quad (6) \\ h(x, y|\zeta, q) = (1-\zeta^2 q^{2i})^2 - (1-q)\zeta q^i (1+\zeta^2 q^{2i})xy \\ + (1-q)\zeta^2 (x^2 + y^2) q^{2i}.$$

The f_{CqN} and f_{biv-qN} are normalized to 1 over the range $s(q)$, which can be inferred from the following property,

$$\int_{s(q)} H_n(x|q) f_{CqN}(x|y; \zeta, q) dx = \zeta^n H_n(y|q). \quad (7)$$

The first four moments of the f_{CqN} can be given [38] as,

$$\begin{aligned} \text{Centroid} &= \zeta y, \\ \text{Variance} &= 1 - \zeta^2, \\ \text{Skewness, } \gamma_1 &= -\frac{\zeta(1-q)y}{\sqrt{1-\zeta^2}}, \\ \text{Excess, } \gamma_2 &= (q-1) + \frac{\zeta^2(1-q)^2 y^2 + \zeta^2(1-q^2)}{(1-\zeta^2)}. \end{aligned} \quad (8)$$

Recently, it is shown that generating function for q -Hermite polynomials describes Gaussian to semi-circle transition in the eigenvalue density as k changes from 1 to m in spectral densities using k -body EGOE and their Unitary variants EGUE, both for fermion and boson systems [33]. Very recently, in the strong coupling domain the lowest four moments of the strength function for k -body fermionic embedded ensemble are obtained and it is shown that they are essentially same as that of f_{CqN} [38]. Therefore, one can use f_{CqN} distribution to represent the smooth forms of the strength functions and analyze the wavefunction structure in quantum many-body systems with k -body interactions. With this, the width of f_{CqN} (and also of the strength function) is related to the correlation coefficient ζ by Eq. (8). In the next section, we will present our results for the variation of parameter q and the correlation coefficient ζ as a function of k -body interaction strength λ in BEGOE(1+k). Also, a complete analytical description of ζ , in terms of N, m, k and λ , for BEGOE(1+k) is given.

3. Parameter dependence of q and ζ : results for BEGOE(1+k)

3.1. Formula of q -parameter

It has already been demonstrated that the state density for EE(k) (and also EE(1+k)) in general exhibits Gaussian to semi-circle transition as k increases from 1 to m [17]. This is now well verified in many numerical calculations and analytical proofs obtained via lower order moments [2,6,9,20,39,43]. Fig. 1(a) represents ensemble averaged state density obtained for a 100 member BEGOE(1+k) ensemble with $m = 10$ bosons distributed in $N = 5$ sp states and the body rank of interaction changing from $k = 2$ to 10. In these calculations, the eigenvalue spectrum for each member of the ensemble is first zero centered (ϵ_H is centroid) and scaled to unit width (σ_H is width) and then the histograms are constructed. The results clearly display transition in the spectral density from Gaussian to semi-circle form as k changes from 2 to $m = 10$. With E as zero centered and using $x = E/\sigma_H$, the numerical results are compared with the normalized state density $\rho(E) = d f_{qN}(x|q)$ with $\epsilon_H - \frac{2\sigma_H}{\sqrt{1-q}} \leq E \leq \epsilon_H + \frac{2\sigma_H}{\sqrt{1-q}}$. Here the parameter q is computed using the formula, valid for BEGOE(k) (i.e. $H = V(k)$), given in [33],

$$q_{V(k)} \sim \binom{N+m-1}{m}^{-1} \sum_{v=0}^{v_{\max}=\min[k, m-k]} \frac{X(N, m, k, v) d(g_v)}{[\Lambda^0(N, m, k)]^2}; \\ X(N, m, k, v) = \Lambda^v(N, m, m-k) \Lambda^v(N, m, k); \quad (9) \\ \Lambda^v(N, m, r) = \binom{m-v}{r} \binom{N+m+v-1}{r}, \\ d(g_v) = \binom{N+v-1}{v}^2 - \binom{N+v-2}{v-1}^2.$$

In the strong coupling domain, one can also apply Eq. (9) to BEGOE(1+k), as the k -body part of the interaction is expected to dominate over one-body part. One can see that the ensemble averaged results in Fig. 1(a) are in excellent agreement with the smooth forms obtained using f_{qN} . With $\lambda = 0$ in Eq. (2) i.e. one-body part $h(1)$ only, the analytical formula of q for bosons, based on trace propagation method [44], can be given as,

$$q_{h(1)} = \frac{\langle h(1)^4 \rangle^m - 2}{\left\{ \frac{3(m-1)N(1+N)(1+m+N)}{m(2+N)(3+N)(m+N)} - 2 \right\} + \frac{m^2 + (N+m)^2 + (N+2m)^2}{m(N+m)} \frac{\sum_{i=1}^N \tilde{\epsilon}_i^4}{(\sum_{i=1}^N \tilde{\epsilon}_i^2)^2}}. \quad (10)$$

Here, $\langle h(1)^4 \rangle^m$ is the reduced fourth moment of one-body part and $\tilde{\epsilon}_i$ are the traceless sp energies of i 'th state. With $H = h(1)$ and uniform sp energies $\epsilon_i = i$, Eq. (10) gives $q = 0.71$ for ($m = 5, N = 10$) and $q = 0.68$ for ($m = 10, N = 5$). While with sp energies $\epsilon_i = i + 1/i$, used in the present study, one obtains $q = 0.68$ for ($m = 5, N = 10$) and $q = 0.63$ for ($m = 10, N = 5$). Fig. 1(b) shows variation of $q_{h(1)}$ as a function of N for various values of m/N . Here, sp energies $\epsilon_i = i + 1/i$ are used. It can be clearly seen that in the dense limit ($m \rightarrow \infty, N \rightarrow \infty$ and $m/N \rightarrow \infty$), $q_{h(1)} \rightarrow 1$. In the dilute limit ($m \rightarrow \infty, N \rightarrow \infty$ and $m/N \rightarrow 0$), similar variation in $q_{h(1)}$ can be observed due to $m \leftrightarrow N$ symmetry between the dense limit and the dilute limit as identified in [18,44]. Furthermore, the variation of parameter q is also studied as the interaction strength λ varies in BEGOE(1+k) for a fixed body rank k . Here, the ensemble averaged value of q is computed for a system of 100 member BEGOE(1+k) ensemble with $m = 10$ bosons in $N = 5$ sp states and results are shown in Fig. 1(c). q estimates are also shown in the figure by horizontal marks for $H = h(1)$ and

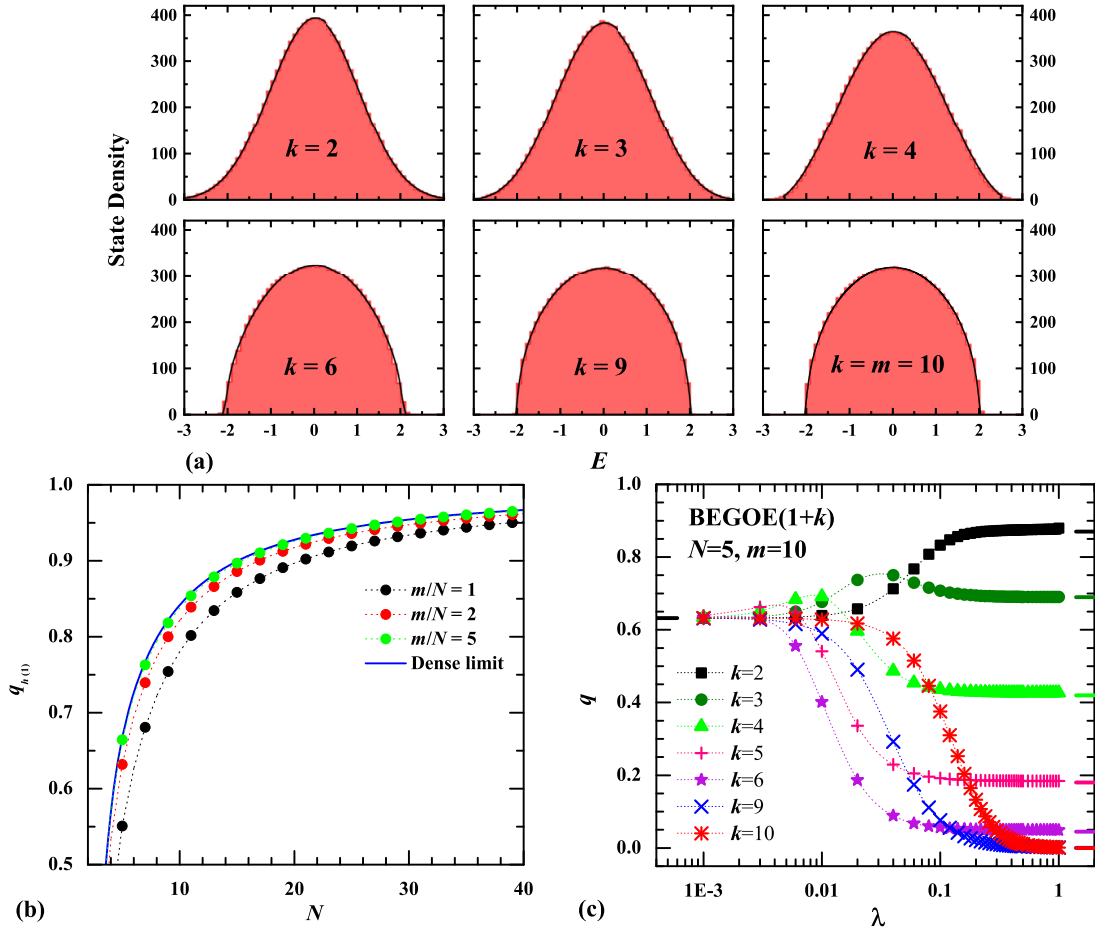


Fig. 1. (a) Histograms represent the state density vs. normalized energy E results of the spectra of a 100 member BEGOE(1+k) ensemble with $m = 10$ bosons in $N = 5$ sp states for different k values. The strength of interaction $\lambda = 0.5$ is chosen and in the plots $\int \rho(E)dE = d$. Ensemble averaged state density histogram is compared with q -normal distribution (continuous black curves) given by $f_{qN}(x|q)$ with the corresponding q values given by Eq. (9). (b) $q_{h(1)}$ vs. N for various values of m/N . $q_{h(1)}$ is obtained using Eq. (10) with sp energies $\epsilon_i = i + 1/i$. Dense limit curve corresponds to the result with $m/N = 1000$. (c) Ensemble averaged q vs. λ for a 100 member BEGOE(1+k) ensemble with $m = 10$ bosons in $N = 5$ sp states for different k values. The horizontal black mark on left q -axis indicates q estimate for $H = h(1)$ given by Eq. (10), while the colored marks on right q -axis represent the q values, given by Eq. (9), for corresponding k -body rank with $H = V(k)$. See text for more details. (For interpretation of the colors in the figures, the reader is referred to the web version of this article.)

$H = V(k)$ on left and right vertical axes respectively. One can see that for very small values of λ , ensemble averaged q values are found very close to $q_{h(1)}$ for all body rank k . While for a sufficiently large λ , where k -body part dominates over one-body part, the ensemble averaged q values reach corresponding $q_{V(k)}$ given by Eq. (9). From the variation of ensemble averaged q values in Fig. 1(c), one can see that the shape of the state density takes intermediate form between Gaussian to semi-circle as λ changes in BEGOE(1+k) for a fixed k . Therefore, the q -normal distribution f_{qN} formula can be used to describe the transition in the state density with any value of λ and k in BEGOE(1+k).

3.2. Formula of ζ

The parameter ζ , which is the correlation coefficient between full Hamiltonian H and the diagonal part H_{dia} of the full Hamiltonian, is related to the width σ_F of the strength functions, given by,

$$\zeta = \sqrt{1 - \frac{\sigma_{H_{\text{off-dia}}}^2}{\sigma_H^2}} = \sqrt{1 - \sigma_F^2}, \quad \sigma_F = \frac{\sigma_{H_{\text{off-dia}}}}{\sigma_H} \quad (11)$$

In the above equation, σ_H^2 and $\sigma_{H_{\text{off-dia}}}^2$ are variances of the eigenvalue distribution using full Hamiltonian and by taking all diagonal

matrix elements as zero, respectively. Since ζ and σ_F are simply related as $\sigma_F^2 = 1 - \zeta^2$, here the discussion is in terms of ζ . For BEGOE(1+k) ensemble, analytical expression for ζ based on the method of trace propagation can be derived as follows. For $H = V(k)$ i.e. with all sp energies as degenerate, it is known that [20],

$$\sigma_{H=V(k)}^2 = T(N, m, k) \binom{N+k-1}{k}^{-1} \sum_{\alpha, \beta} \overline{w_{\alpha\beta}^2}, \quad (12)$$

$$T(N, m, k) = \Lambda^0(N, m, k) / \binom{N+k-1}{k}.$$

Here, α and β denote k -particle states. In k -particle space, the H matrix is GOE. Therefore, the k -particle matrix elements $w_{\alpha\beta}$ are Gaussian random variates with zero mean and unit variance. The variance of diagonal matrix elements is $\overline{w_{\alpha\alpha}^2} = 2$ while that of off-diagonal matrix elements is $\overline{w_{\alpha\beta}^2} = 1$ for $(\alpha \neq \beta)$. With this,

$$\sigma_{H=V(k)}^2 = T(N, m, k) \binom{N+k-1}{k}^{-1} \times \{2 \times \text{no-dia} + 2 \times \text{no-offdia}\}, \quad (13)$$

here the number of independent diagonal k -body matrix elements is 'no-dia' = $\binom{N+k-1}{k}$ and that of off-diagonal is 'no-offdia' =

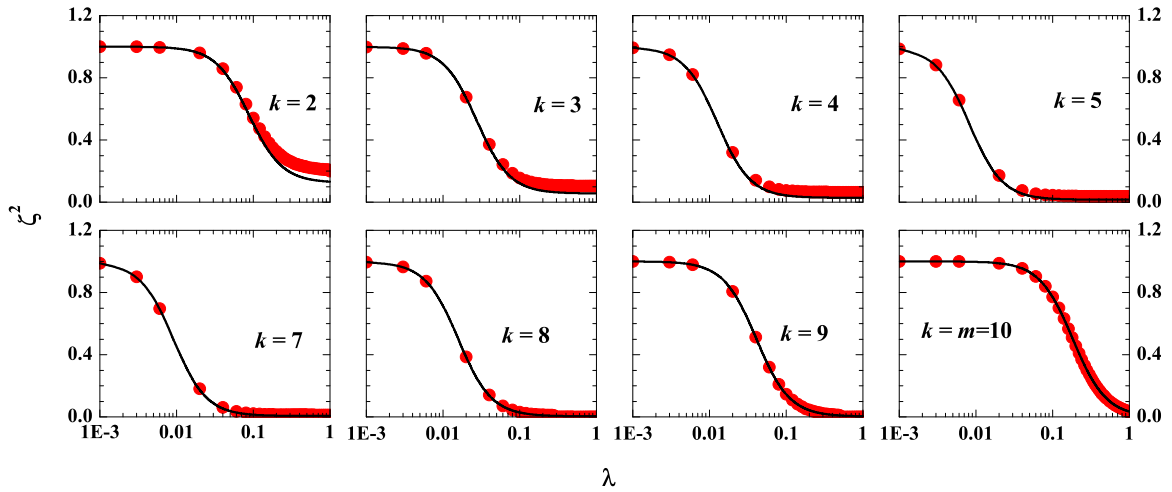


Fig. 2. Ensemble averaged ζ^2 (red solid circles) as a function of interaction strength λ , calculated for BEGOE(1+k) ensemble with $N = 5, m = 10$ example, is shown for different k values. The smooth black curves are due to Eq. (16) using fixed sp energies $\epsilon_i = i + 1/i$ employed in the present study.

$\frac{1}{2} \binom{N+k-1}{k} \{ \binom{N+k-1}{k} - 1 \}$. Similarly, $\sigma_{H_{\text{off-dia}}}$ is given by removing the contribution of diagonal k -body matrix elements from the above equation. Then using Eq. (11) for $H = V(k)$,

$$\zeta^2 = \frac{4}{\binom{N+k-1}{k} + 1}. \quad (14)$$

Here, it can be immediately seen that ζ^2 is independent of m for BEGOE(k). In the dense limit with $N \rightarrow \infty$ and $m \rightarrow \infty$, $\sigma_F \rightarrow 1$ giving $\zeta \rightarrow 0$ as was suggested in [21]. Also, with $k \ll m$, $\zeta^2 \propto 1/N^k$. Using $m \leftrightarrow N$ symmetry between the dense limit and the dilute limit formula [18,44], we have $\zeta^2 \propto 1/m^k$ in the dilute limit and this result is in agreement with [38]. Going further, with inclusion of one-body part defined by the external sp energies (ϵ_i), and with $H = h(1) + \lambda V(k)$, we have

$$\begin{aligned} \sigma_H^2 &= \sigma_{h(1)}^2 + \lambda^2 \sigma_{V(k)}^2, \\ &= \frac{m(N+m)}{N(N+1)} \sum \tilde{\epsilon}_i^2 + \lambda^2 \sigma_{V(k)}^2. \end{aligned} \quad (15)$$

The analytical expression for ζ^2 can be given by,

$$\zeta^2 = \frac{\frac{m(N+m)}{N(N+1)} \sum \tilde{\epsilon}_i^2 + 2\lambda^2 T(N, m, k)}{\frac{m(N+m)}{N(N+1)} \sum \tilde{\epsilon}_i^2 + \lambda^2 T(N, m, k) \{ 1 + \binom{N+k-1}{k} \}}. \quad (16)$$

In the above equation, the contribution from the diagonal part of $V(k)$ is also included into the numerator term. The analytical expression for ζ^2 given by Eq. (16) is tested with the numerical ensemble averaged results obtained using a 100 member BEGOE(1+k) ensemble with ($m = 10, N = 5$). The results of ζ^2 as a function of k -body interaction strength λ for different body rank k are presented in Fig. 2. The black smooth curve in each plot is obtained using Eq. (16) with fixed sp energies employed in the present study. It can be seen from the results that agreement between the ensemble averaged values (red solid circles) and the smooth forms obtained by Eq. (16) is very good for all k values. Small difference with large λ , for $k < 5$, is due to neglect of induced sp energies. The contribution of induced sp energies reduces as λ and k increases. One can see from the results shown in Fig. 2 that the width of the strength function is strongly dependent on λ . For $\lambda \rightarrow 0$, $\zeta^2 \rightarrow 1$ for all k and the strength functions are known to be represented by δ functions. With increase in λ i.e. $\lambda \geq \lambda_C$, the strength functions are known to be described by the Briet-Wigner (Lorentz) form. With further increase in $\lambda \gg \lambda_F$, ζ^2 goes on decreasing smoothly leading to a fully chaotic domain giving the Gaussian or semi-circle or intermediate to Gaussian and

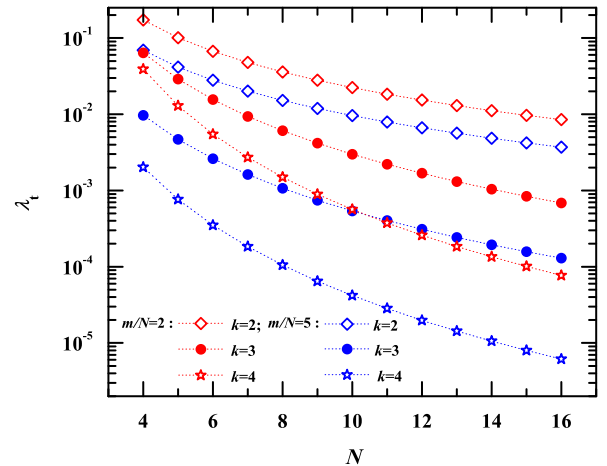


Fig. 3. Variation of marker λ_t as a function of N for dense boson systems with BEGOE(1+k). Results are shown for various values of ($k, m/N$) using Eq. (17).

semi-circle character of the strength functions depending upon the values of λ and k . One can also observe the BW to Gaussian to semi-circle transition in strength functions by changing both λ and k . Therefore, it is possible to have a shape intermediate to BW and semi-circle for some values of λ and k [45].

For two-body interaction, the thermodynamic region $\lambda = \lambda_t$ can be determined using the condition $\zeta^2 = 0.5$ [23,46]; i.e. the spreading produced by one-body part and two-body part are equal. Similarly, one can obtain marker λ_t for k -body interactions in presence of mean field by considering the spreading produced by one-body part and k -body part equal in Eq. (16). Solving it for λ , (m, N, k) dependence of marker λ_t is given by,

$$\lambda_t = \sqrt{\frac{m(N+m) \sum \tilde{\epsilon}_i^2}{N(N+1) \Lambda^0(N, m, k) (1 - 3 \binom{N+k-1}{k}^{-1})}}. \quad (17)$$

Fig. 3 shows the variation of marker λ_t in dense boson systems with BEGOE(1+k) as a function of N for the fixed sp energies used in the present study. The results are shown for body rank values $k = 2, 3$ and 4 , and with $m/N = 2$ and 5 . From the results one can clearly see that λ_t decreases as the rank of the interaction k increases. Hence, the thermalization sets in faster as the rank of interaction k increases.

Recently, using k -body embedded ensembles both for fermions and bosons, it is demonstrated that in the thermalization region ($\lambda \geq \lambda_t$), shape of the strength functions changes from Gaussian to semi-circle for the states close to the center of the spectrum as the rank of the interaction k increases and they can be well represented by f_{qN} form for all k values in $V(k)$ [33]. The strength functions are symmetrical in E near the center of the spectrum as is the result with f_{qN} . However, it is seen in some calculations with $k = 2$ that the strength functions become asymmetrical in E as one moves away from the center [24]. This feature can be incorporated by representing strength function using f_{CqN} which can not be generated by f_{qN} . This will be verified with a numerical example in the next section and more importantly, a single interpolating function f_{CqN} , in terms of parameters q and ζ , is considered for describing Gaussian to semi-circle transition in the strong coupling domain as the body rank k in BEGOE(1+k) is changed.

4. Strength function

Given m -particle basis state $|\kappa\rangle$, the diagonal matrix elements of m -particle Hamiltonian H are denoted as energy ξ_κ , so that $\xi_\kappa = \langle \kappa | H | \kappa \rangle$. The diagonalization of the full matrix H gives the eigenstates $|E_i\rangle$ with eigenvalues E_i , where $|\kappa\rangle = \sum_i C_\kappa^i |E_i\rangle$. The strength function that corresponds to the state $|\kappa\rangle$ is defined as $F_{\xi_\kappa}(E) = \sum_i |C_\kappa^i|^2 \delta(E - E_i)$. In the present study, we take the $|\kappa\rangle$ states to be the eigenstates of $h(1)$. In order to get an ensemble averaged form of the strength functions, the eigenvalues E_i are scaled to have zero centroid and unit variance for the eigenvalue distribution. The κ -energies, ξ_κ , are also scaled similarly. Now, for each member, all $|C_\kappa^i|^2$ are summed over the basis states κ with energy ξ in the energy window $\xi \pm \Delta$. Then, the ensemble averaged $F_\xi(E)$ vs. E are constructed as histograms by applying the normalization condition $\int_{s(q)} F_\xi(E) dE = 1$. In Fig. 4, histograms represent ensemble averaged $F_\xi(E)$ results for all body rank k values with $\lambda = 0.5$ using a 250 member BEGOE(1+k) ensemble with $m = 10$ and $N = 5$ system. The strength function plots are obtained for $\xi = 0.0, \pm 1.0$ and ± 2.0 . The value of k -body interaction strength is chosen such that $\lambda \gg \lambda_t$, i.e. the system exists in the region of thermalization [9,23]. The histograms, representing BEGOE(1+k) results of strength functions, are compared with the conditional q -normal density function as given by,

$$F_\xi(E) = f_{CqN}(x = E | y = \xi; \zeta, q). \quad (18)$$

The smooth black curves in Fig. 4 for each k are obtained via Eq. (18) using corresponding ensemble averaged ζ and q values. With $\lambda \gg \lambda_t$, $\zeta^2 \ll 1/2$, the q value in Eq. (18) can fairly be given by Eq. (9) [38]. The results in Fig. 4 clearly show very good agreement between the numerical histograms and continuous black curves for all body rank k . The $F_\xi(E)$ results for $\xi = 0$ are given in Fig. 4(a) which clearly demonstrate that the strength functions are symmetric and also exhibit a transition from Gaussian form to semi-circle as k changes from 2 to $m = 10$. The smooth form given by Eq. (18) using the conditional q -normal density function interpolates this transition very well. Going further, $F_\xi(E)$ results for $\xi \neq 0$ are shown in Figs. 4(b) and 4(c). One can see that $F_\xi(E)$ results are asymmetrical about E as demonstrated earlier [24]. Also, $F_\xi(E)$ are skewed more in the positive direction for $\xi > 0$ and skewed more in the negative direction for $\xi < 0$ and their centroids vary linearly with ξ . We have also computed the first four moments (centroid, variance, skewness (γ_1) and excess (γ_2)) of the strength function results shown in Fig. 4 for the body rank k going from 2 to $m = 10$. Fig. 5 represents results for centroid, γ_1 and γ_2 for various values of ξ . As discussed earlier in Section 3, the variance of the strength functions is independent of ξ and simply related to correlation

coefficient; for more details, see results of ζ^2 (Fig. 2). From the numerical results obtained for strength functions (Fig. 4) along with results of lower order moments (Fig. 5), one can clearly see that in the thermodynamic domain, the strength functions of dense interacting many-boson systems, with k -body interaction, follow the conditional q -normal distribution f_{CqN} . The results are also consistent with the analytical forms derived in [38].

In the study of thermalization and relaxation dynamics of an isolated finite quantum system after a random interaction quench, strength functions play an important role. Having tested that in the thermodynamic region with $\lambda \gg \lambda_t$, ensemble averaged strength functions of dense boson systems with k -body interaction can be represented by smooth forms given by f_{CqN} , we will now utilize these interpolating forms, in the coming sections, to study fidelity decay and NPC in dense boson systems with k -body interaction.

5. Fidelity decay after an interaction quench

Fidelity decay or return probability of a quantum system after a sudden quench is an important quantity in the study of relaxation of a complex (chaotic) system to an equilibrium state. Let's say the system is prepared in one of the eigenstates ($\psi(0) = |\kappa\rangle$) of the mean-field Hamiltonian $H = h(1)$. With the quench at $t = 0$ by $\lambda V(k)$, the system evolves unitarily with respect to $H \rightarrow h(1) + \lambda V(k)$ and the state changes after time t to $\psi(t) = |\kappa(t)\rangle = \exp(-iHt) |\kappa\rangle$. Then, the probability to find the system in its initial unperturbed state after time t , called fidelity decay, is given by,

$$\begin{aligned} W_0(t) &= |\langle \psi(t) | \psi(0) \rangle|^2 = \left| \sum_E [C_k^E]^2 \exp -iEt \right|^2 \\ &= \int F_\xi(E) \exp -iEt dE \\ &= \int_{s(q)} f_{CqN}(E | \xi; \zeta, q) \exp -iEt dE. \end{aligned} \quad (19)$$

Thus, fidelity decay is the Fourier transform in energy of the strength function; this is valid for times not very short or very long. In the thermalization region, the form of $F_\xi(E)$ is Gaussian for $k = 2$ while it is semi-circle for $k = m$. These two extreme situations are recently studied, both analytically [47] as well as numerically [48–50]. The formula for $W_0(t)$ can be given in terms of width of $\lambda V(k)$ scaled by σ_H . Clearly, following the results of the previous section, f_{CqN} can be used to obtain $W_0(t)$ generated by BEGOE(1+k). As analytical formula for the Fourier transform of f_{CqN} is not available, therefore we evaluated Eq. (19) numerically. Fig. 6 shows results for $W_0(t)$ (red solid circles) for a 100 member BEGOE(1+k) ensemble with $m = 10$, $N = 5$ and $\lambda = 0.5$ for various k values and they are compared with numerical Fourier transform (black smooth curves) of Eq. (18). Here, we have used normalized eigenenergies in the computation of W_0 and therefore the time t is measured in the units of $1/\sigma_H$. It is clear from the results that the Fourier transform of f_{CqN} describes the short-time behavior nicely and also captures the positions of the oscillations. The results generated here are consistent with the reported results in [33], obtained using f_{qN} form for $F_\xi(E)$.

It is known that in the strong interaction domain, the decrease in W_0 (for $k = 2$) follows quadratic in time and this Gaussian decrease can last for a quite large time and after that an exponential one emerges [51]. The transition time depends on the ratio of the spectral width and the square of the second moment of strength function (σ_F^2). As here $\lambda \gg \lambda_t$, $\zeta^2 \rightarrow 0$ giving $\sigma_F^2 \approx 1$, t is in $1/\sigma_H$ units and the spectral width will be in σ_H units. Therefore, the results in Fig. 6 describe W_0 nicely for short time and the standard exponential decrease for long time for $k = 2$ seems absent. The long time behavior of fidelity decay is of great interest as it is expected that W_0 surely demonstrates a power-law behavior i.e.

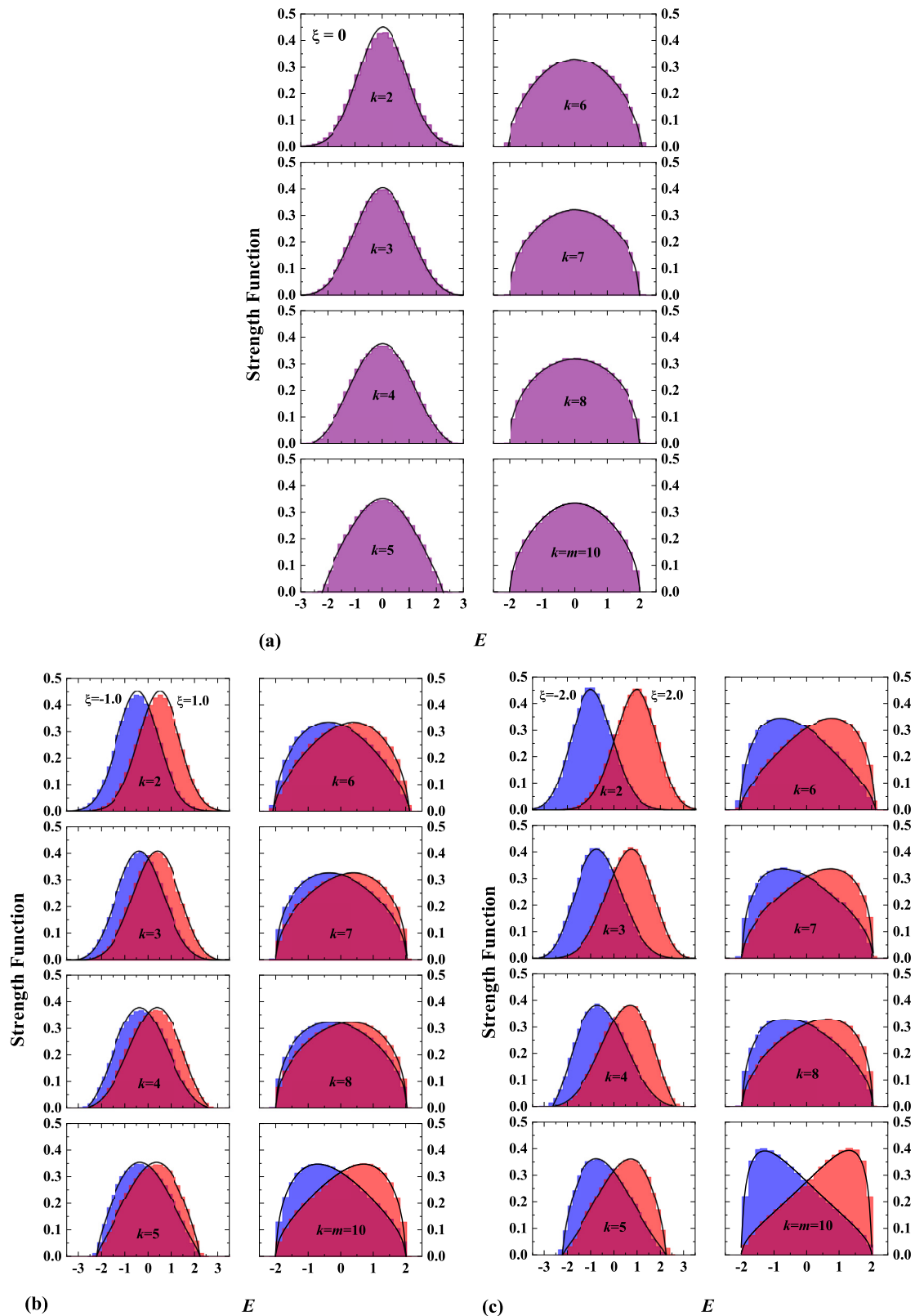


Fig. 4. Strength function vs. normalized energy E for a system of $m = 10$ bosons in $N = 5$ sp states with $\lambda = 0.5$ for different k values in BEGOE(1+k) ensemble. An ensemble of 250 members is used for each k . Strength function plots are obtained for (a) $\xi = 0$ (purple histogram), (b) $\xi = -1.0$ (blue histogram) and 1.0 (red histogram) and (c) $\xi = -2.0$ (blue histogram) and 2.0 (red histogram). In the plots $\int F_{\xi}(E)dE = 1$. The continuous black curves are due to fitting with f_{CqN} given by Eq. (18) using q and ζ values obtained by Eq. (9) and Eq. (11), respectively. See text for more details.

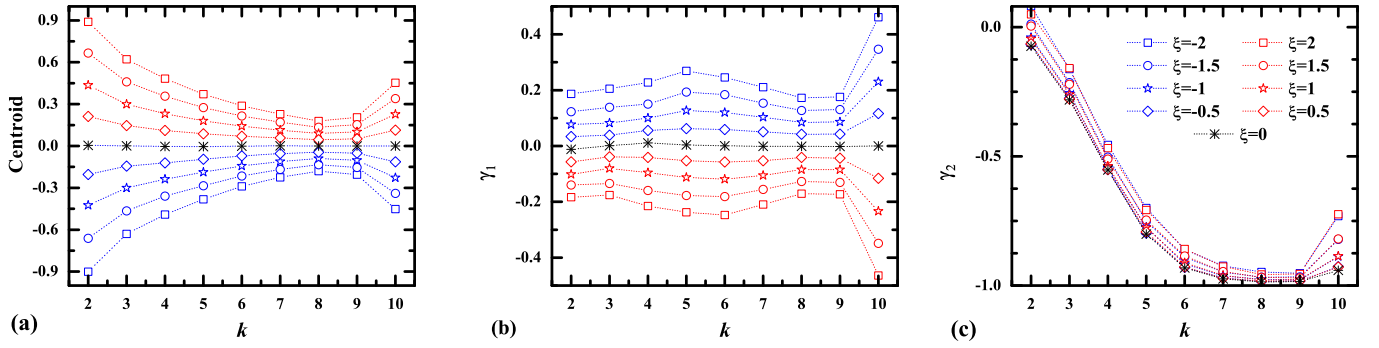


Fig. 5. Ensemble averaged (a) Centroid, (b) γ_1 and (c) γ_2 as a function of body rank k for the strength function results presented in Fig. 4. Results are shown for various values of ξ .

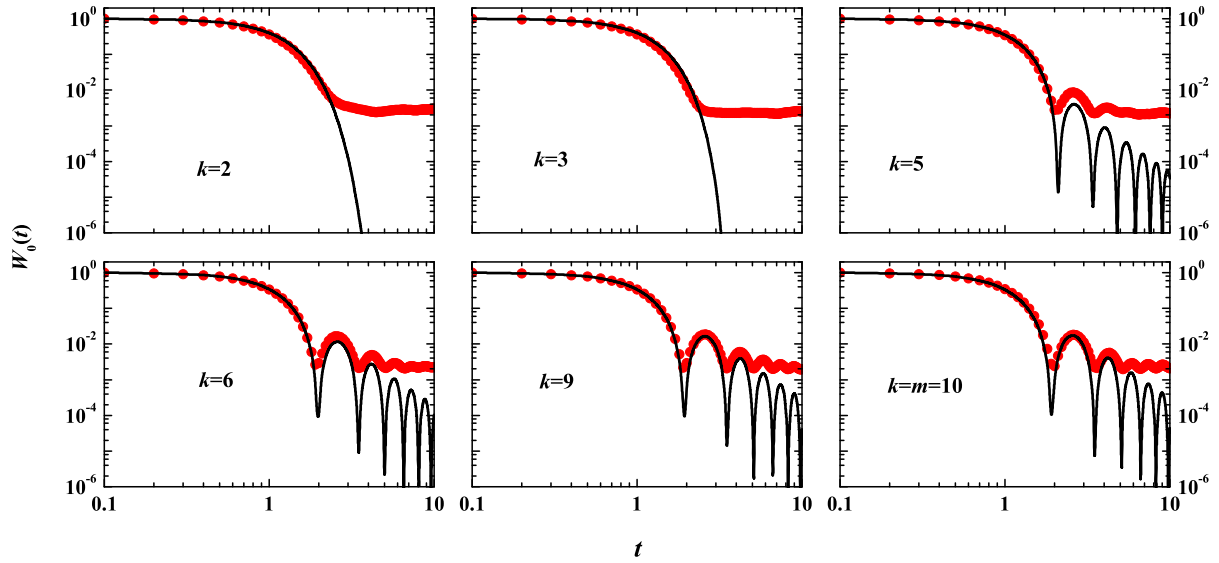


Fig. 6. Fidelity decay $W_0(t)$ as a function of time for a 100 member BEGOE(1+k) ensemble with $N = 5$ and $m = 10$ represented by the red solid circles; the $\psi(0)$ here corresponds to middle states of $h(1)$ spectrum. Here t is measured in the units of σ_H^{-1} . The black smooth curves are obtained by taking numerical Fourier transform of the strength functions represented by Eq. (18).

$W_0(t) \propto t^{-\gamma}$ with $\gamma \geq 2$ implying thermalization [52], no matter how fast the decay may initially be. As shown in [52], the power-law behavior appears due to the fact that the energy spectrum is bounded from both the ends. This condition is essentially satisfied by f_{CqN} . Therefore, it is important to analyze the long-time behavior of fidelity decay for embedded ensembles first to establish its universality and second to test whether it can be explained with the use of f_{CqN} . These are open questions.

In the study of fidelity decay, strength function with $\xi = 0$ is involved. However, the statistical properties, related to wavefunction structure, namely NPC and S^{info} can be written as integrals involving strength functions over all ξ energies. Very recently, an integral formula for NPC in the transition strengths from a state as a function of energy for fermionic EGOE(k) using the bivariate q -normal form is presented in [37]. In the past, the smooth forms, for NPC and S^{info} , were derived in terms of energy and correlation coefficient ζ for two-body interaction [53]. In the next section, we present our results for NPC and S^{info} using f_{CqN} forms for the strength functions and compare with those for dense interacting boson systems with k -body interaction.

6. NPC and information entropy

The NPC in wavefunction characterizes various layers of chaos in interacting particle systems [16,54,55] and for a system like atomic nuclei, NPC for transition strengths is a measure of fluctua-

tions in transition strength sums [37]. For an eigenstate $|E_i\rangle$ spread over the basis states $|\kappa\rangle$, with energies $\xi_\kappa = \langle \kappa | H | \kappa \rangle$, NPC (also known as inverse participation ratio) is defined as,

$$\text{NPC}(E) = \left\{ \sum_{\kappa} |c_{\kappa}^i|^4 \right\}^{-1} \quad (20)$$

NPC essentially gives the number of basis states $|\kappa\rangle$ that constitute an eigenstate with energy E . The GOE value for NPC is $d/3$. NPC can be studied by examining the general features of the strength functions $F_{\xi}(E)$. The smooth forms for NPC(E) can be written as [53],

$$\text{NPC}(E) = \frac{d}{3} \left\{ \int d\xi \frac{\rho^{H_{\kappa}}(\xi) [F_{\xi}(E)]^2}{[\rho^H(E)]^2} \right\}^{-1}, \quad (21)$$

where $\rho^{H_{\kappa}}(\xi)$ and $\rho^H(E)$ are normalized eigenvalue densities generated by diagonal Hamiltonian H_{κ} matrix and full Hamiltonian H matrix, respectively. Taking E and ξ as zero centered and scaled by corresponding widths, the above equation can be written in terms of f_{qN} and f_{CqN} [37,38],

$$\text{NPC}(E) = \frac{d}{3} \left\{ \int_{s(q)} d\xi \frac{f_{qN}(\xi|q) [f_{CqN}(E|\xi; \zeta, q)]^2}{f_{qN}(E|q)} \right\}^{-1}. \quad (22)$$

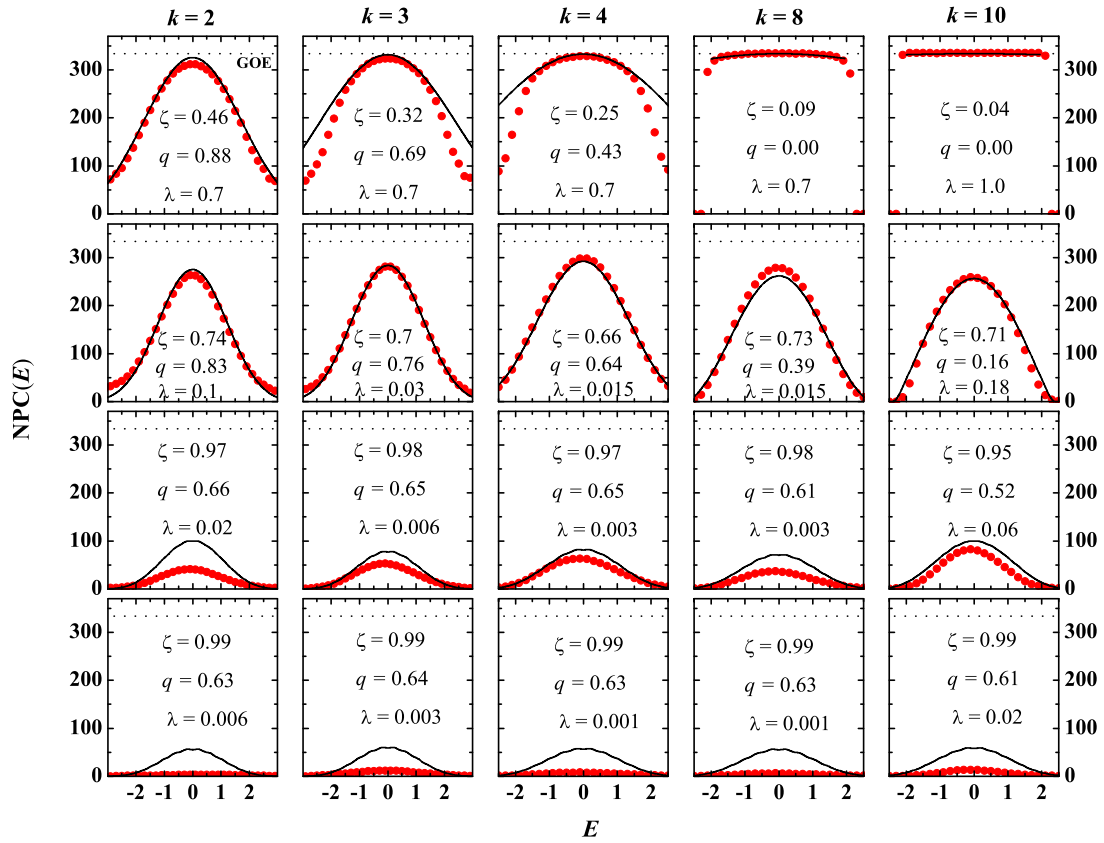


Fig. 7. Ensemble averaged NPC as a function of normalized energy E for a 100 member BEGOE(1+k) with $m = 10$ interacting bosons in $N = 5$ sp states for different values of k . Ensemble averaged BEGOE(1+k) results are represented by solid circles while continuous curves correspond to the theoretical estimates in the chaotic domain obtained using Eq. (23). The ensemble averaged ζ and q values are also given in the figure. GOE estimate is represented by dotted line in each graph.

In general, q 's in the above equation need not be same [37,38]. However, in the thermalization region, with $\zeta^2 \leq 1/2$, one can approximate $\gamma_2 \approx (q - 1)$ in Eq. (8). Then, the formula for q given by Eq. (9) is valid for f_{qN} as well as for f_{CqN} . This is well verified numerically in Section 2. Also, the results of γ_2 in Fig. 5(c) corroborate this claim. With this, it is possible to simplify Eq. (22) using Eqs. (6) and (7) and a simple two-parameter formula, valid in chaotic domain, for NPC can be written as,

$$\text{NPC}(E) = \frac{d}{3} \left\{ \sum_{n=0}^{\infty} \frac{\zeta^{2n}}{[n]_q!} H_n^2(E|q) \right\}^{-1}. \quad (23)$$

It is easy to see from above formula that $\text{NPC}(E)$ approaches GOE value $d/3$ as $\zeta \rightarrow 0$. Also for $q \rightarrow 1$, f_{qN} and f_{CqN} in Eq. (22) reduce to Gaussian and then Eq. (23) gives similar results obtained for $k = 2$ in [53]. We have tested this formula with numerical ensemble averaged BEGOE(1+k) results. Fig. 7 shows results for ensemble averaged NPC vs. normalized energy, for a 100 member BEGOE(1+k) with $m = 10$ and $N = 5$ example for different values of λ and k . The ensemble averaged NPC values are shown with red solid circles and continuous lines are obtained using the theoretical expression given by Eq. (23). One can see from the results that with fixed k (i) for small value of λ , where the one-body part of the interaction is dominating, the numerical NPC values are zero and the theoretical curve is far away from the numerical results indicating that the wavefunctions are completely localized (the bottom panels in Fig. 7); (ii) with further increase in λ , the theoretical estimate for NPC in the chaotic domain is much above the ensemble averaged curve indicating that the chaos has not yet set in; (iii) However, with sufficiently large λ , we see that the ensemble averaged curve is matching with the theoretical estimate

given by Eq. (23), indicating that system is in chaotic domain corresponding to the thermalization region given by $\zeta^2 \sim 1/2$ [23] and the strength functions $F_{\xi}(E)$ are well represented by conditional q normal distribution. Again with further increase in λ (the top panels in Fig. 7), the match between the theoretical chaotic domain estimate and the ensemble averaged values is very well in the bulk part of the spectrum ($|E| < 2$) for all values of k with deviations near the spectrum tails. Hence, in the chaotic domain, the energy variation of $\text{NPC}(E)$ using Eq. (23) is essentially given by two parameters, ζ and q . The results clearly show that the thermalization sets in faster with increase in the body rank k .

Another statistical quantity normally considered is the information entropy defined by $S^{\text{info}}(E) = -\sum_{\kappa} p_{\kappa}^i \ln p_{\kappa}^i = -\sum_{\kappa} |C_{\kappa}^i|^2 \ln |C_{\kappa}^i|^2$, here p_{κ}^i is the probability of basis state κ in the eigenstate at energy E_i . The localization length, l_H is related to $S^{\text{info}}(E)$ by $l_H(E) = \exp\{S^{\text{info}}(E)\}/(0.48d)$. Then the corresponding embedded ensemble expression for l_H involving $F_{\xi}(E)$, can be written as [53],

$$l_H(E) = - \int d\xi \frac{F_{\xi}(E) \rho^{H_{\kappa}}(\xi)}{\rho^H(E)} \ln \left\{ \frac{F_{\xi}(E)}{\rho^H(E)} \right\}. \quad (24)$$

Replacing $\rho^{H_{\kappa}}(\xi)$ and $\rho^H(E)$ by f_{qN} and $F_{\xi}(E)$ by f_{CqN} , formula for l_H valid in chaotic domain is given by,

$$l_H(E) = - \int d\xi \int_{s(q)} \frac{f_{CqN}(E|\xi; \zeta, q) f_{qN}(\xi|q)}{f_{qN}(E|q)} \ln \left\{ \frac{f_{CqN}(E|\xi; \zeta, q)}{f_{qN}(E|q)} \right\}. \quad (25)$$

Simplifying Eq. (25) for l_H is an open problem and therefore, it is evaluated numerically and results are compared with ensemble

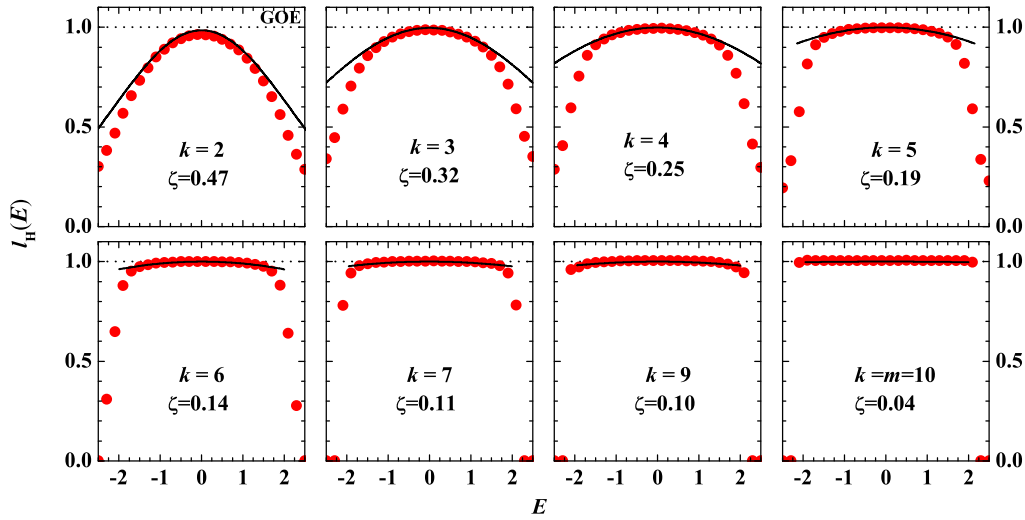


Fig. 8. Ensemble averaged localization lengths l_H vs. normalized energy E for a 100 member BEGOE(1+k) with $m = 10$ interacting bosons in $N = 5$ sp states for different k values. Here, $\lambda = 1$ is chosen for all k . Ensemble averaged BEGOE(1+k) results (red solid circles) are compared with the smooth forms obtained via Eq. (25) involving parameters ζ and q . The ensemble averaged ζ values are given in the figure and Eq. (9) is used for q values. Dotted lines in each graph represent GOE estimate.

averaged numerical results of BEGOE(1+k). Fig. 8 shows results for ensemble averaged l_H vs. normalized energy E for a 100 member BEGOE(1+k) with $m = 10$ bosons in $N = 5$ sp states for different values of k . Here, we choose k -body interaction strength $\lambda = 1$ so that the system will be in thermalization region. Numerical embedded ensemble results (red solid circles) are compared with theoretical estimates (black curves) obtained using Eq. (25). The ζ values are shown in the figure. A very good agreement between numerical results and smooth form is obtained for all values of k in the bulk of the spectrum with small deviations near the spectrum tails. Hence, in the chaotic domain, the energy variation of $l_H(E)$, with Eq. (25), is essentially given by conditional q forms for the strength functions.

7. Conclusions

In the present work, we have analyzed wavefunction structure of dense many-body bosonic systems with k -body interaction by modeling the Hamiltonian of these complex systems using BEGOE(1+k). We have shown that for dense boson systems with BEGOE(1+k), the q -Hermite polynomials are used to describe the transition from Gaussian to semi-circle in the state density as the strength of the k -body interaction increases. A complete analytical description of the correlation coefficient ζ , which is related to variance of strength functions, is obtained in terms of N , m , k and λ and it is found to describe the embedded ensemble results very well for all the values of rank of interaction k . Also, in the dense limit $\zeta \rightarrow 0$. We have also obtained formula for λ_t in terms of (m, N, k) . Further, it is shown that in the strong interaction domain ($\lambda \gg \lambda_t$), the strength functions make transition from Gaussian to semi-circle as the rank of interaction k increases in BEGOE(1+k) and their smooth forms can be represented by the q -normal distribution function f_{CqN} to describe this crossover. Moreover, the variations of the lowest four moments of strength functions computed numerically are in good agreement with the analytical formulas obtained in [38]. With this, we have first utilized the interpolating form for strength function f_{CqN} to describe the fidelity decay in dense boson systems after k -body random interaction quench. Secondly, using smooth forms for f_{qN} and f_{CqN} , we have also derived two-parameter (q and ζ) formula for NPC valid in thermalization region and shown that these smooth forms describe BEGOE(1+k) ensemble averaged results very well. Therefore, the results of this work, along with [33,37,38], establish that

the q -Hermite polynomials play a very significant role in analyzing many-body quantum systems interacting via k -body interaction. The generic features explored in this work are important for a complete description of many-body quantum systems interacting via k -body interaction as the nuclear interactions are now known to have some small 3-body and 4-body parts and higher body interactions may become prominent in strongly interacting quantum systems [7,25,26].

Following the work in [52], it is interesting to analyze power-law behavior of fidelity decay for very long time using embedded ensembles with k -body forces as smooth forms of strength functions can be represented by f_{CqN} . Further, as smooth forms for the density of states can be represented by f_{qN} , it is possible to study normal mode decomposition of the density of states for various k values using f_{qN} [13,17,56] and thereby one can study spectral statistics in strongly interacting quantum systems. This is for future. It is also known that the strength functions and the entanglement essentially capture the same information about eigenvector structure [55,57] and therefore it is important to study entanglement properties using embedded ensembles with k -body forces.

CRediT authorship contribution statement

All authors contributed equally and agreed to the published version of the manuscript.

Declaration of competing interest

The authors declare that they have no known competing financial interests or personal relationships that could have appeared to influence the work reported in this paper.

Acknowledgements

Thanks are due to Manan Vyas for collaboration in the initial stages of this work and V. K. B. Kota for many useful discussions. Authors acknowledge support from Department of Science and Technology (DST), Government of India [Project No.: EMR/2016/001327]. NDC acknowledges support from the International Centre for Theoretical Sciences (ICTS) during a visit for participating in the program - Thermalization, Many body localization and Hydrodynamics (Code: ICTS/hydrodynamics2019/11).

References

- [1] O. Bohigas, M.J. Giannoni, C. Schmit, *Phys. Rev. Lett.* **52** (1984) 1.
- [2] V.K.B. Kota, *Embedded Random Matrix Ensembles in Quantum Physics*, Springer-Verlag, Heidelberg, 2014.
- [3] A. Polkovnikov, K. Sengupta, A. Silva, *Rev. Mod. Phys.* **83** (2011) 863.
- [4] L. D'Alessio, Y. Kafri, A. Polkovnikov, M. Rigol, *Adv. Phys.* **65** (2016) 239.
- [5] F. Borgonovi, F.M. Izrailev, L.F. Santos, V.G. Zelevinsky, *Phys. Rep.* **626** (2016) 1.
- [6] V.K.B. Kota, N.D. Chavda, *Int. J. Mod. Phys. E* **27** (2018) 1830001.
- [7] J.S. Cotler, et al., *J. High Energy Phys.* **05** (2017) 118.
- [8] J.J.M. Verbaarschot, *Quantum chromodynamics*, in: G. Akemann, J. Baik, P. Di Francesco (Eds.), *The Oxford Handbook of Random Matrix Theory*, Oxford University Press, Oxford, 2011.
- [9] V.K.B. Kota, N.D. Chavda, *Entropy* **20** (2018) 541.
- [10] J.B. French, S.S.M. Wong, *Phys. Lett. B* **33** (1970) 449.
- [11] O. Bohigas, J. Flores, *Phys. Lett. B* **34** (1971) 261.
- [12] V.K.B. Kota, *Phys. Rep.* **347** (2001) 223.
- [13] T.A. Brody, J. Flores, J.B. French, P.A. Mello, A. Pandey, S.S.M. Wong, *Rev. Mod. Phys.* **53** (1981) 385.
- [14] T. Papenbrock, H.A. Weidenmüller, *Rev. Mod. Phys.* **79** (2007) 997.
- [15] V.V. Flambaum, G.F. Gribakin, F.M. Izrailev, *Phys. Rev. E* **53** (1996) 5729.
- [16] V.V. Flambaum, F.M. Izrailev, *Phys. Rev. E* **56** (1997) 5144.
- [17] K.K. Mon, J.B. French, *Ann. Phys. (N.Y.)* **95** (1975) 90.
- [18] K. Patel, M.S. Desai, V. Potbhare, V.K.B. Kota, *Phys. Lett. A* **275** (2000) 329.
- [19] T. Asaga, L. Benet, T. Rupp, H.A. Weidenmüller, *Europhys. Lett.* **56** (2001) 340.
- [20] T. Asaga, L. Benet, T. Rupp, H.A. Weidenmüller, *Ann. Phys. (N.Y.)* **298** (2002) 229.
- [21] N.D. Chavda, V. Potbhare, V.K.B. Kota, *Phys. Lett. A* **311** (2003) 331.
- [22] N.D. Chavda, V. Potbhare, V.K.B. Kota, *Phys. Lett. A* **326** (2004) 47.
- [23] N.D. Chavda, V.K.B. Kota, V. Potbhare, *Phys. Lett. A* **376** (2012) 2972.
- [24] N.D. Chavda, V.K.B. Kota, *Ann. Phys. (Berlin)* **529** (2017) 1600287.
- [25] D.W.E. Blatt, B.H.J. McKellar, *Phys. Rev. C* **11** (1975) 2040.
- [26] H-W. Hammer, A. Nogga, A. Schwenk, *Rev. Mod. Phys.* **85** (2013) 197.
- [27] K.D. Launey, T. Dytrych, J.P. Draayer, *Phys. Rev. C* **85** (2012) 044003.
- [28] A.M. Garcia-Garcia, Y. Jia, J.J.M. Verbaarschot, *Phys. Rev. D* **97** (2018) 106003.
- [29] A.M. Garcia-Garcia, T. Nosaka, D. Rosa, J.J.M. Verbaarschot, *Phys. Rev. D* **100** (2019) 026002.
- [30] A. Ortega, M. Vyas, L. Benet, *Ann. Phys. (Berlin)* **527** (2015) 748.
- [31] A. Ortega, T. Stegmann, L. Benet, *Phys. Rev. E* **94** (2016) 042102.
- [32] A. Ortega, T. Stegmann, L. Benet, *Phys. Rev. E* **98** (2018) 012141.
- [33] M. Vyas, V.K.B. Kota, *J. Stat. Mech. Theory Exp.* **10** (2019) 103103.
- [34] A.M. Garcia-Garcia, J.J.M. Verbaarschot, *Phys. Rev. D* **94** (2016) 126010, *Phys. Rev. D* **96** (2017) 066012.
- [35] Y. Jia, J.J.M. Verbaarschot, *J. High Energy Phys.* **07** (2020) 193.
- [36] L. Erdos, D. Schroder, *Math. Phys. Anal. Geom.* **17** (2014) 441.
- [37] V.K.B. Kota, M. Vyas, arXiv:2003.09191v1.
- [38] V.K.B. Kota, M. Vyas, arXiv:2011.05799v1.
- [39] L. Benet, T. Rupp, H.A. Weidenmüller, *Ann. Phys. (N.Y.)* **292** (2001) 67.
- [40] M. Vyas, T.H. Seligman, *AIP Conf. Proc.* **1950** (2018) 030009.
- [41] M.E.H. Ismail, D. Stanton, G. Viennot, *Eur. J. Comb.* **8** (1987) 379.
- [42] P. Szablowski, *Electron. J. Probab.* **15** (2010) 1296.
- [43] R.A. Small, S. Müller, *Ann. Phys. (N.Y.)* **356** (2015) 269.
- [44] V.K.B. Kota, V. Potbhare, *Phys. Rev. C* **21** (1980) 2637.
- [45] B. Lauritzen, P.F. Bortignon, R.A. Broglia, V.G. Zelevinsky, *Phys. Rev. Lett.* **74** (1995) 5190.
- [46] D. Angom, S. Ghosh, V.K.B. Kota, *Phys. Rev. E* **70** (2004) 016209.
- [47] S.K. Haldar, N.D. Chavda, M. Vyas, V.K.B. Kota, *J. Stat. Mech. Theory Exp.* **2016** (2016) 043101.
- [48] E.J. Torres-Herrera, M. Vyas, L.F. Santos, *New J. Phys.* **16** (2014) 063010.
- [49] E.J. Torres-Herrera, J. Karp, M. Tavora, L.F. Santos, *Entropy* **18** (2016) 359.
- [50] L.F. Santos, E.J. Torres-Herrera, *AIP Conf. Proc.* **1912** (2017) 020015.
- [51] M. Schiulaz, E.J. Torres-Herrera, L.F. Santos, *Phys. Rev. B* **99** (2019) 174313.
- [52] M. Tavora, E.J. Torres-Herrera, L.F. Santos, *Phys. Rev. A* **95** (2017) 013604.
- [53] V.K.B. Kota, R. Sahu, *Phys. Rev. E* **64** (2001) 016219.
- [54] P.G. Silvestrov, *Phys. Rev. E* **58** (1998) 5629.
- [55] C. Mejia-Monasterio, J. Richert, T. Rupp, H.A. Weidenmüller, *Phys. Rev. Lett.* **81** (1998) 5189.
- [56] R.J. Leclair, R.U. Haq, V.K.B. Kota, N.D. Chavda, *Phys. Lett. A* **372** (2008) 4373.
- [57] W.G. Brown, L.F. Santos, D.J. Starling, L. Viola, *Phys. Rev. E* **77** (2008) 021106.



Ordered level spacing distribution in embedded random matrix ensembles

PRIYANKA RAO^{1,*}, H N DEOTA²  and N D CHAVDA¹ 

¹Department of Applied Physics, Faculty of Technology and Engineering, The Maharaja Sayajirao University of Baroda, Vadodara 390001, India

²HVHP Institute of Post Graduate Studies and Research, Kadi Sarva Vishwavidyalaya, Gandhinagar 382715, India

*Corresponding author. E-mail: pnao-apphy@msubaroda.ac.in

MS received 2 July 2020; revised 29 September 2020; accepted 21 October 2020

Abstract. The probability distributions of the closest neighbour (CN) and farther neighbour (FN) spacings from a given level have been studied for interacting fermion/boson systems with and without spin degree of freedom constructed using an embedded Gaussian orthogonal ensemble (GOE) of one plus random two-body interactions. Our numerical results demonstrate a very good consistency with the recently derived analytical expressions using a 3×3 random matrix model and other related quantities by Srivastava *et al*, *J. Phys. A: Math. Theor.* **52**, 025101 (2019). This establishes conclusively that local level fluctuations generated by embedded ensembles (EE) follow the results of classical Gaussian ensembles.

Keywords. Level fluctuations; spacing distribution; finite interacting particle systems; embedded ensembles.

PACS Nos 05.40.–a; 05.45.Mt; 05.30.Fk; 05.30.Jp

1. Introduction

Random matrix theory (RMT) originally introduced by Wishart [1] in statistics and further introduced by Wigner to study nuclear spectra [2], is now established as a good model to describe spectral fluctuations arising from complex quantum systems from a wide variety of fields like quantum chaos, finance [3], econophysics [4], quantum chromodynamics [5], functional brain structures [6] and many more. These spectral fluctuations reveal whether the given complex quantum system is in regular (or integrable) or chaotic domain and they describe transition from regular to chaotic domain. One of the most popular measure of RMT widely used for this purpose is the nearest-neighbour spacing distribution (NNSD), $P(s)$, which tells us about the short-range correlations between nearest neighbours of energy levels (or eigenvalues) of the complex quantum system. Dyson gave three-fold classification of classical random matrix ensembles based on the symmetries present in their Hamiltonian, viz. Gaussian orthogonal ensemble (GOE), Gaussian unitary ensemble (GUE) and Gaussian symplectic ensemble (GSE) [7]. For the case of GOE, which corresponds to quantum systems that are time reversal invariant without spin, the energy levels

are correlated (corresponding to the chaotic behaviour) and NNSD obeys the Wigner surmise which is essentially the GOE result $P(s) = (\pi/2)s \exp(-\pi s^2/4)$ [8], whereas if the energy levels of a complex quantum system are uncorrelated (corresponding to the regular behaviour), then the form of NNSD is given by the Poisson distribution $P(s) = \exp(-s)$ [9]. For a given set of energy levels, the construction of NNSD involves unfolding of the spectra to remove the variation in the density of eigenvalues [7, 10]. Recently, NNSD has been used to study this transition from regular to chaotic domain in wormholes [11] and open quantum systems [12].

Complex systems can be represented in the form of a network and the spectral properties of these networks are now known to follow RMT. This opened a route to predict and control functional behaviour of these complex systems [13, 14]. In some complex systems such as cancer networks, the short-range correlations given by NNSD may give information only about the random connections in these networks. However, the long-range correlations given by spectral rigidity can give further details about the underlying structural patterns in these systems [15]. In such systems, study of measures giving long-range correlations, such as the number variance

and spectral rigidity, are important [10,16–18]. These days, a very good alternative to NNSD called the ratio of level spacings [19] is gaining a lot of attention [15,20–24] as it is simple to compute and no unfolding is needed as it is independent of the form of density of the energy levels. The higher orders of ratio of spacings have also been studied in [25,26]. The distribution intermediate of Poisson and GOE is described by Brody distribution [27]. Recently, intermediate semi-Poissonian statistics [28] and cross-over random matrix ensembles [29] are also reported. Going beyond this, recently, the distribution of the closest neighbour (CN) spacing, s_{CN} , and farther neighbour (FN) spacing, s_{FN} , from a given level are introduced [30]. The distribution of s_{CN} is important in the context of perturbation theory, as the contribution from the CN is prominent due to smaller energy spacing [31]. The distribution of s_{FN} is complementary to that of s_{CN} . It is important to note that the ratio of two consecutive level spacings introduced in [19] is given by $\tilde{r} = s_{\text{CN}}/s_{\text{FN}}$. The numerical results for the integrable circle billiard, fully chaotic cardioid billiard, standard map with chaotic dynamics and broken time reversal symmetry, and the zeros of the Riemann zeta function are shown to be in very good agreement with the analytical formulas derived in [30] for the random matrix ensembles GOE, GUE and GSE based on a 3×3 matrix modelling and Poisson spectra. In the present work, we analyse distributions of s_{CN} and s_{FN} using random matrix ensembles defined by one-plus chaos generating two-body interactions operating in many-particle spaces, to conclusively establish that these measures are universal and local level fluctuations generated by many-particle interacting systems follow the results of classical Gaussian ensembles [32–34]. These ensembles are generically called the embedded ensembles of $(1+2)$ -body interactions or simply EE $(1+2)$ and their GOE random matrix version is called EGOE $(1+2)$. These models, both for fermion and boson systems, including spin degree of freedom and without spin, have their origin in nuclear shell model and the interacting boson model [35].

Now, it is very well established that EGOE $(1+2)$ ensembles apply in a generic way to isolated finite interacting many-particle quantum systems such as nuclei, atoms, quantum dots, small metallic grains, interacting spin systems modelling quantum computing core and so on [33,36]. For sufficiently strong interaction, EGOEs exhibit average-fluctuation separation in eigenvalues with the smoothed eigenvalue density being a corrected Gaussian and the local fluctuations are of GOE type [10,34,37]. Recently, these models have also been used successfully in understanding high-energy physics related problems. Random matrix models with two-body interactions [EGOE (2)] among complex fermions

are known as complex Sachdev–Ye–Kitaev models in this area [38–40]. EGOE $(1+2)$ can be defined for fermions and bosons with spin degree of freedom and also with many other symmetries [34,36]. Now we shall give a preview.

The rest of this paper is organised as follows. In §2, we briefly describe the construction of five different EGOEs used in the present paper. Analytical results for the probability distribution for the CN spacings and the FN spacings are discussed in §3. Section 4 presents the numerical results for the probability distribution for the CN spacings and the FN spacings. Finally, we draw conclusions in §5.

2. Embedded ensembles for fermion and boson systems

In this section, we describe the construction of various embedded random matrix ensembles used in this paper. Let us begin with embedded ensemble (EE) for spinless systems. For defining such ensembles, one can consider a system of m spinless particles (fermions or bosons) which are to be distributed in N single particle (sp) states and interacting via $(1+2)$ body interaction. Let these N sp states be denoted by $|v_i\rangle$ where $i = 1, 2, 3, \dots, N$. A two-particle Hamiltonian matrix can be constructed and then it can be further embedded to the m -particle space by using the concepts of direct product space and Lie algebra. With GOE embedding, these ensembles are called EGOE (2) for fermions (or BEGOE (2) for bosons). For such a system, one can define the two-body Hamiltonian matrix by the expression

$$V(2) = \sum_{\alpha,\gamma} V_{2;\alpha,\gamma} A_{2,\alpha}^\dagger A_{2,\gamma}, \quad (1)$$

where the term $V_{2;\alpha,\gamma}$ is the Gaussian random variate with zero mean and constant variance,

$$\overline{V_{2;\alpha,\gamma} V_{2;\alpha',\gamma'}} = v_0^2 (1 + \delta_{\alpha,\alpha',\gamma,\gamma'}), \quad (2)$$

where the overbar denotes the ensemble average and $v_0 = 1$ without the loss of generality. For fermions, $A_{2,\alpha}^\dagger = a_{v_1}^\dagger a_{v_2}^\dagger$; $A_{2,\alpha} = (A_{2,\alpha}^\dagger)^\dagger$ ($v_1 < v_2$), whereas for bosons, $A_{2,\alpha}^\dagger = C b_{v_1}^\dagger b_{v_2}^\dagger$; $A_{2,\alpha} = (A_{2,\alpha}^\dagger)^\dagger$ ($v_1 \leq v_2$), where C is the normalisation constant given by $C = (1 + \delta_{v_1 v_2})^{-1/2}$ and α simplifies the notation of indices. Also, $a_{v_i}^\dagger$ and a_{v_i} are the creation and annihilation operators respectively for fermions and $b_{v_i}^\dagger$ and b_{v_i} are the creation and annihilation operators respectively for bosons. One should also note that the dimension of Hamiltonian matrix for fermions would be $d(N, m) = \binom{N}{m}$ and for bosons $d(N, m) = \binom{N+m-1}{m}$, with the

two-body independent matrix elements (TBME) being $[d(N, 2)(d(N, 2) + 1)]/2$ for both. $V_{2;\alpha,\gamma}$ in eq. (1), are anti-symmetrised TBME for fermions and symmetrised TBME for bosons.

In such a manner, one can construct an embedded two-body random matrix ensemble. When the mean field one-body part is added to the Hamiltonian, they are generally called one plus two-body random matrix ensembles [EGOE(1 + 2)]. Thus, with random two-body interactions $V(2)$, we can define the Hamiltonian of EGOE(1 + 2) as follows:

$$H = h(1) + \lambda\{V(2)\}. \tag{3}$$

Here, $h(1) = \sum_i \epsilon_i n_i$ is the one-body part of the Hamiltonian. The sp energies are defined as ϵ_i and n_i are number operators acting on sp states. λ is the two-body interaction strength and notation $\{ \}$ denotes an ensemble. The $V(2)$ matrix is chosen to be a GOE in two-particle spaces [36]. Due to (1 + 2)-body nature of the interaction, many of the matrix elements of $H(m)$ for $m > 2$ are zero and the non-zero matrix elements are linear combinations of the sp energies and the TBMEs.

Going beyond spinless systems, we have considered three embedded ensembles (EE) with spin degree of freedom. For fermions with spin $s = 1/2$ degree of freedom, we have EGOE(1 + 2)-s [41]. Here, the interaction $V(2)$ will have two parts as the two-particle spins are $s = 0$ and 1, giving EGOE(1 + 2)-s Hamiltonian $H = h(1) + \lambda_0\{V^{s=0}(2)\} + \lambda_1\{V^{s=1}(2)\}$. For bosons with spin degree of freedom, we have considered the following two EE: (i) for two-species boson systems with a fictitious (F) spin $1/2$ degree of freedom, we have BEGOE(1 + 2)- F [42]. Here also, the interaction $V(2)$ will have two parts as the two-particle F spins are $f = 0$ and 1, giving BEGOE(1 + 2)- F Hamiltonian $H = h(1) + \lambda_0\{V^{f=0}(2)\} + \lambda_1\{V^{f=1}(2)\}$, (ii) for bosons with spin-one degree of freedom, we have BEGOE(1 + 2)- $S1$ [43]. Here, the interaction $V(2)$ will have three parts as the two-particle spins are $s = 0, 1$ and 2 giving BEGOE(1 + 2)- $S1$ Hamiltonian $H = h(1) + \lambda_0\{V^{s=0}(2)\} + \lambda_1\{V^{s=1}(2)\} + \lambda_2\{V^{s=2}(2)\}$. Note that, the sp levels (Ω) defining one-body part $h(1)$ for EE will have $(2s + 1)$ degeneracy. For EGOE(1 + 2)-s and BEGOE(1 + 2)- F , the sp levels will be doubly degenerate ($N = 2\Omega$), while for BEGOE(1 + 2)- $S1$, they will be triply degenerate ($N = 3\Omega$). In all the five ensembles, without loss of generality, we choose the average spacing between the sp levels to be unity so that all strength of interactions are unitless.

3. Ordered level spacing distribution

Let us consider an ordered set of unfolded eigenvalues (energy levels) E_n , where $n = 1, 2, \dots, d$. The nearest-neighbour spacing is given by $s_n = E_{n+1} - E_n$. Then, the CN spacing is defined as $s_n^{CN} = \min\{s_{n+1}, s_n\}$ and the FN spacing is defined as $s_n^{FN} = \max\{s_{n+1}, s_n\}$. The probability distribution for the CN spacings is denoted by $P_{CN}(s)$ and for the FN spacings it is denoted by $P_{FN}(s)$. If the system is in integrable domain, NNSD is Poisson. Then $P_{CN}(s)$ and $P_{FN}(s)$ are given by

$$P_{CN}^P(s) = 2 \exp(-2s) \tag{4}$$

and

$$P_{FN}^P(s) = 2 \exp(-s)[1 - \exp(-s)], \tag{5}$$

respectively. Similarly, if the system is in chaotic domain, NNSD is GOE and is derived using 3×3 real symmetric matrices. Then $P_{CN}(s)$ and $P_{FN}(s)$ are given by [30],

$$P_{CN}^{GOE}(s) = \frac{a}{\pi} s \exp(-2as^2) \times \left[3\sqrt{6\pi a} s - \pi \exp\left(\frac{3a}{2}s^2\right) \times (as^2 - 3) \operatorname{erfc}\left(\sqrt{\frac{3a}{2}} s\right) \right] \tag{6}$$

and

$$P_{FN}^{GOE}(s) = \frac{a}{\pi} s \exp(-2as^2) \left[\pi \exp\left(\frac{3a}{2}s^2\right) \times (as^2 - 3) \left\{ \operatorname{erf}\left(\sqrt{\frac{a}{6}} s\right) - \operatorname{erf}\left(\sqrt{\frac{3a}{2}} s\right) \right\} + \sqrt{6\pi a} s \left(\exp\left(\frac{4a}{3}s^2\right) - 3 \right) \right] \tag{7}$$

respectively. Here $a = 27/8\pi$. It is important to note that $2P(s) = P_{CN}(s) + P_{FN}(s)$. For small spacings s , $P_{CN}^{GOE}(s)$ shows level repulsion similar to the NNSD and $P_{FN}^{GOE}(s) \propto s^4$, while for large s , $P_{FN}^{GOE}(s) \propto \exp(-\frac{2a}{3}s^2)$. For GOE, the average value $\langle s_{CN} \rangle = \frac{2}{3}$ and for Poisson it is $\frac{1}{2}$. However, the average value $\langle s_{FN} \rangle = \frac{4}{3}$ for GOE and $\frac{3}{2}$ for Poisson.

Here, spectral fluctuations in EE for fermion and boson systems with and without spin degree of freedom are studied using P_{CN} and P_{FN} and it is found that these forms of distributions are universal. Let us add that the ensembles without spin and with spin degree of freedom are used to represent the quantum many-particle systems with interactions [36]. We present the numerical results in the next section.

Table 1. The ensemble averaged skewness γ_1 and excess γ_2 parameters for various EE examples used.

EE	γ_1	γ_2
EGOE(1 + 2)	0.0008	-0.3431
BEGOE(1 + 2)	0.0922	-0.2329
EGOE(1 + 2)-s		
$S = 0$	0.0202	-0.3034
$S = 1$	0.0178	-0.3352
BEGOE(1 + 2)- F		
$F = 0$	0.0088	-0.3114
$F = 2$	0.0469	-0.3129
$F = 5$	0.0677	-0.2569
BEGOE(1 + 2)- $S1$		
$S = 4$	0.0349	-0.1111

4. Numerical results

In order to study CN spacing distribution $P_{CN}(s)$ and FN spacing distribution $P_{FN}(s)$, we consider the following five EGOEs in many-particle spaces:

1. EGOE(1 + 2) for $m = 6$ fermions in $N = 12$ sp states with H matrix of dimension 924. The interaction strength $\lambda = 0.1$ (see ref. [32] for details).
2. BEGOE(1 + 2) for $m = 10$ bosons in $N = 5$ sp states with H matrix of dimension 1001. The interaction strength $\lambda = 0.06$ (see refs [44,45] for details).
3. EGOE(1 + 2)-s for $m = 6$ fermions occupying $\Omega = 8$ sp levels (each doubly degenerate) with total spin $S = 0$ and $S = 1$ giving the H matrices of dimensions 1176 and 1512 respectively. The interaction strength $\lambda = \lambda_0 = \lambda_1 = 0.1$ (see refs [41,46]) for details).

4. BEGOE(1 + 2)- F for $m = 10$ bosons occupying $\Omega = 4$ sp levels (each doubly degenerate) with total F -spin $F = 0, 2$ and $F = F_{\max} = 5$ giving the H matrices of dimensions 196, 750 and 286. The interaction strength $\lambda = \lambda_0 = \lambda_1 = 0.08$ (see refs [42,47] for details).
5. BEGOE(1 + 2)- $S1$ for $m = 8$ bosons occupying $\Omega = 4$ sp levels (each triply degenerate) with total spin $S = 4$ giving the H matrix of dimension 1841. The interaction strength $\lambda = \lambda_0 = \lambda_1 = \lambda_2 = 0.2$ (see ref. [43] for details).

In the present analysis, an ensemble of 500 members is used for all the examples. The sp energies defining $h(1)$ are chosen as $\epsilon_i = (i + 1/i)$. It is important to note that as λ increases in these EE (both fermion and boson), there is Poisson to GOE transition in level fluctuations at $\lambda = \lambda_C$ and Breit–Wigner to Gaussian transition in strength functions (also known as local density of states) at $\lambda = \lambda_F > \lambda_C$. Also, they generate a third chaos marker at $\lambda = \lambda_t > \lambda_F$, a point or a region where thermalisation occurs. Values of λ in the ensemble calculations are chosen sufficiently large so that there is enough mixing among the basis states and the system is in the Gaussian domain, i.e. $\lambda > \lambda_F$. For EGOE(1 + 2) [32] and EGOE(1 + 2)-s [41,46], fermion systems are always in Gaussian domain with $\lambda = 0.1$. For spinless boson BEGOE(1 + 2), $\lambda = 0.06$ is sufficiently large so that the system is in Gaussian domain [44,45]. Similarly, for boson ensembles with spin degree, BEGOE(1 + 2)- F with $\lambda = 0.08$ [42,47] and BEGOE(1 + 2)- $S1$ with $\lambda = 0.2$ [43], again the systems exhibit GOE level fluctuations and the eigenvalue density as well as strength functions are close to Gaussian.

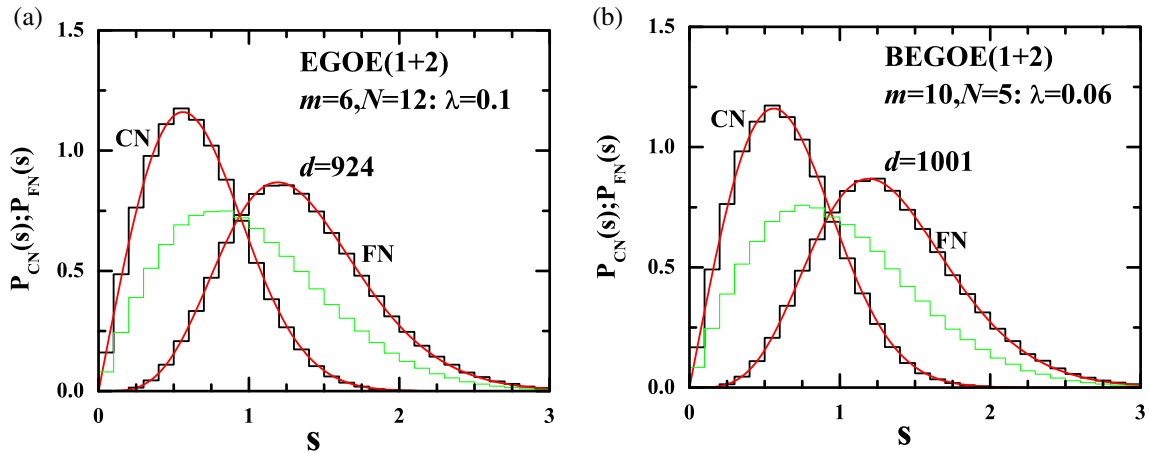


Figure 1. The CN spacing distribution $P_{CN}(s)$ and FN spacing distribution $P_{FN}(s)$ (black histograms) for a 500 member (a) EGOE(1 + 2) ensemble and (b) BEGOE(1 + 2) ensemble. The red smooth curves are due to the corresponding eqs (6) and (7). The NNNSD is shown by the green histogram for comparison.

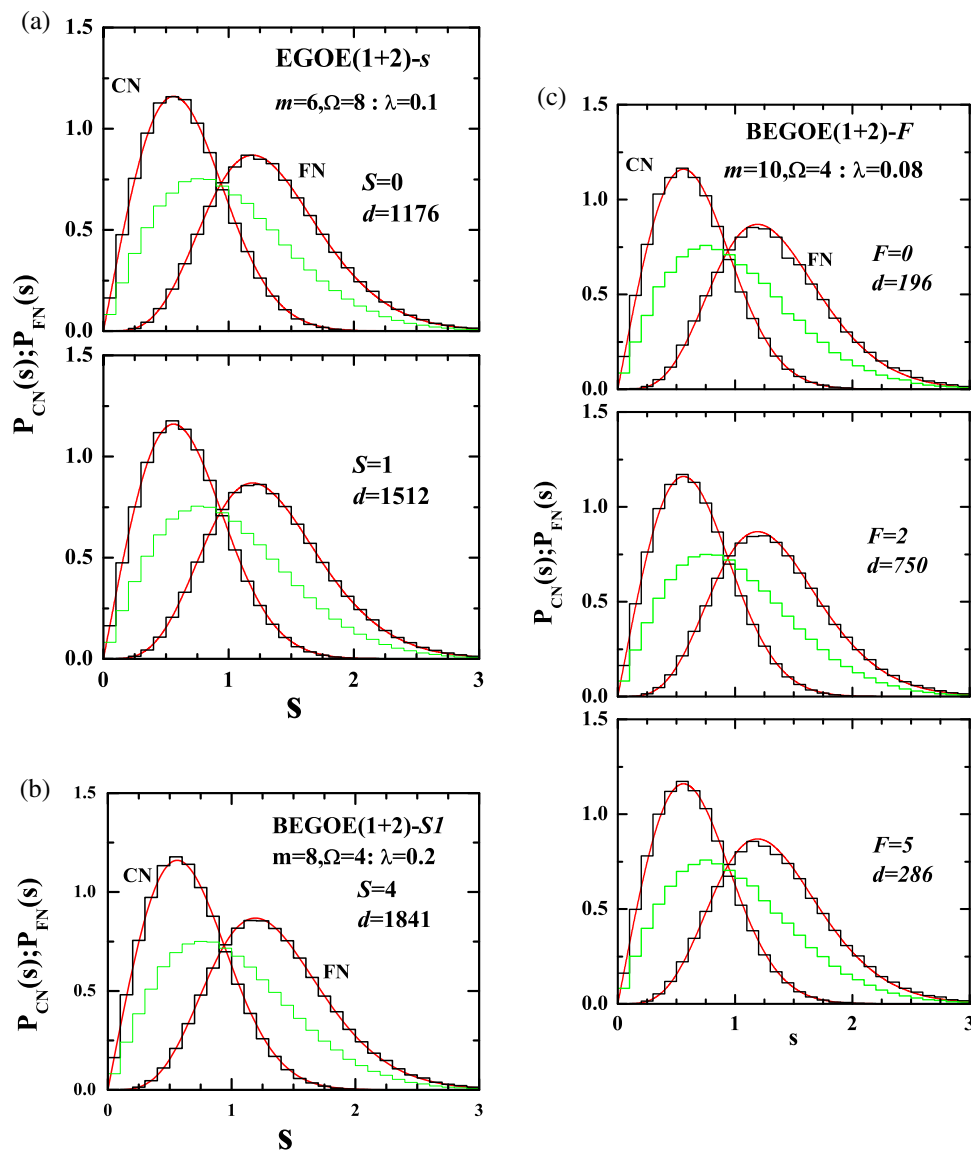


Figure 2. The CN spacing distribution $P_{CN}(s)$ and FN spacing distribution $P_{FN}(s)$ for (a) EGOE(1 + 2)-s ensemble for spin values $S = 0$ and 1, (b) BEGOE(1 + 2)-S1 ensemble for spin value $S = 4$ and (c) BEGOE(1 + 2)-F ensemble for spin values $F = 0, 2$ and 5 (see figure 1 and text for details).

In the analysis, $P_{CN}(s)$ and $P_{FN}(s)$ are obtained using the following procedure. First the spectrum for each member of the ensemble is unfolded using the procedure described in [37], with the smooth density as a corrected Gaussian with corrections involving up to 4–6th order moments of the density function so that the average spacing is unity. The ensemble averaged skewness (γ_1) and excess (γ_2) parameters are shown in table 1 for all the examples of EE analysed in the present work. The histograms for $P_{CN}(s)$ and $P_{FN}(s)$ are constructed using the central 80% part of the spectrum with the bin size equal to 0.1. The results for EE without

spin, EGOE(1 + 2) and BEGOE(1 + 2), are shown in figure 1. Similarly, the results for EE with spin degree of freedom, EGOE(1 + 2)-s and BEGOE(1 + 2)-F and BEGOE(1 + 2)-S1, are shown in figure 2. A very good agreement is observed between the numerical EE results and the theoretical predictions given by eqs (6) and (7) for all the examples. The ensemble averaged values of $\langle s_{CN} \rangle$ and $\langle s_{FN} \rangle$, for all the examples, are given in table 2. They are found to be very close to the corresponding GOE estimates. In addition to this, we have also analysed shell model example which is a typical member of EGOE(1 + 2)-JT [32]. This ensemble is usually called

Table 2. Average values of the CN spacings ($\langle s_{\text{CN}} \rangle$) and FN spacing ($\langle s_{\text{FN}} \rangle$) obtained numerically for various EE examples used in the present paper. Average values obtained from theory for Poisson and GOE are also given.

EE	$\langle s_{\text{CN}} \rangle$	$\langle s_{\text{FN}} \rangle$
EGOE(1 + 2)	0.6613	1.3417
BEGOE(1 + 2)	0.6600	1.3401
EGOE(1 + 2)-s		
$S = 0$	0.6616	1.3411
$S = 1$	0.6625	1.3409
BEGOE(1 + 2)-F		
$F = 0$	0.6585	1.3421
$F = 2$	0.6600	1.3404
$F = 5$	0.6578	1.3420
BEGOE(1 + 2)-S1		
$S = 4$	0.6600	1.3401
Poisson	1/2	3/2
GOE	2/3	4/3

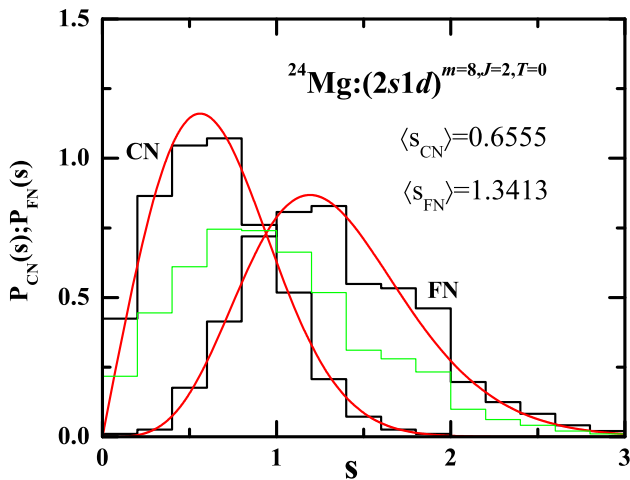


Figure 3. The CN spacing distribution $P_{\text{CN}}(s)$ and FN spacing distribution $P_{\text{FN}}(s)$ vs. s for nuclear shell model example: ^{24}Mg with 8 nucleons in the $(2s1d)$ shell with angular momentum $J = 2$ and isospin $T = 0$. The matrix dimension is 1206 and all levels are used in the analysis (see ref. [37] for further details). The skewness and excess parameters are $\gamma_1 = 0.139$ and $\gamma_2 = -0.061$. $\langle s_{\text{CN}} \rangle$ and $\langle s_{\text{FN}} \rangle$ values are also given in the figure.

TBRE [48]. The result is shown in figure 3. Here also the shell model results along with the calculated averages are consistent with the theoretical predictions.

Going further, it is also possible to study a transition from Poisson to GOE in terms of $\langle s_{\text{CN}} \rangle$ and $\langle s_{\text{FN}} \rangle$ for EGOE(1 + 2) and BEGOE(1 + 2) ensembles as these ensembles demonstrate Poisson to GOE transition in level fluctuations with increase in the strength of the two-body interaction λ [22,32,42,44,46]. We have computed $\langle s_{\text{CN}} \rangle$ and $\langle s_{\text{FN}} \rangle$ for spinless fermion and boson ensembles by varying the interaction strength λ .

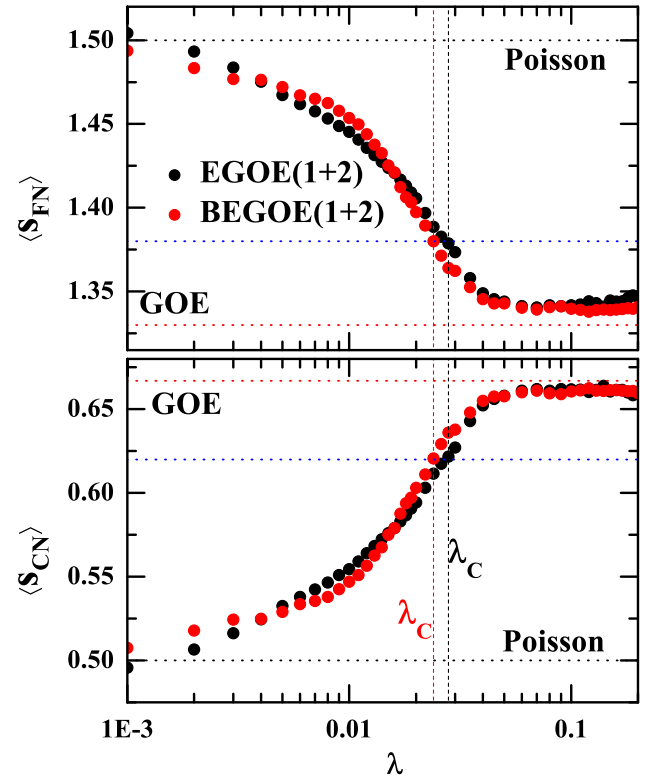


Figure 4. Ensemble averaged values of $\langle s_{\text{CN}} \rangle$ (lower panel) and $\langle s_{\text{FN}} \rangle$ (upper panel) as a function of the two-body strength of interaction λ , obtained for EGOE(1 + 2) ensemble with $(m, N) = (6, 12)$ (black circles) and BEGOE(1 + 2) ensemble with $(m, N) = (10, 5)$ (red circles). In the calculations sp energies are drawn from the centre of a GOE. The vertical dash lines represent the position of λ_C for the corresponding EGOE(1 + 2) and BEGOE(1 + 2) examples. In each calculation, an ensemble of 500 members is used. The horizontal dotted lines represent Poisson estimate (black), GOE estimate (red) and $\langle s_{\text{CN}} \rangle_C = 0.62$ (and $\langle s_{\text{FN}} \rangle_C = 1.38$) (see text for further details).

Figure 4 represents these results. It is clearly seen that for lower values of λ , the values of $\langle s_{\text{CN}} \rangle$ and $\langle s_{\text{FN}} \rangle$ are close to Poisson, which gradually reach the GOE value with increase in λ . Therefore, there is a transition from Poisson to GOE form in $P_{\text{CN}}(s)$ (and also in $P_{\text{FN}}(s)$). With this, it is possible to define a chaos marker λ_C such that for $\lambda > \lambda_C$, the level fluctuations follow GOE. This transition occurs when the interaction strength λ is of the order of the spacing Δ between the states that are directly coupled by the two-body interaction. In the past, the NNSD [49] and the distribution of ratio of consecutive level spacings [21] have been used to study Poisson-to-GOE transition by constructing suitable random matrix model and the transition parameters were used to identify the chaos marker λ_C in the EE [22,32,42,44,46]. Corresponding to the critical values of these transition parameters required for the onset of GOE fluctuations, we found the critical value of $\langle s_{\text{CN}} \rangle$,

$\langle s_{\text{CN}} \rangle_C = 0.62$ (and $\langle s_{\text{FN}} \rangle_C = 1.38$). This is represented by blue dotted lines in figure 4. $\langle s_{\text{CN}} \rangle_C = 0.62$ gives $\lambda_C \simeq 0.028$ for EGOE(1+2) example and $\lambda_C \simeq 0.024$ for BEGOE(1+2) example. These values are shown by dashed vertical lines in figure 4 and are close to the previously obtained results [22,36]. Therefore, these measures can also be utilised to identify λ_C marker using $P_{\text{CN}}(s)$. In the past, the criterion for the chaos marker λ_C for EGOE(1+2) models [36,44], based on the perturbation theory, was derived by Jacquod and Shepelyansky [50]. The validity of the perturbation theory gives λ_C . Hence, it is important to analyse $P_{\text{CN}}(s)$ distribution and related measures in the context of the onset of chaos in EE. This is for future.

5. Conclusion

In this paper, we have studied the CN spacing distribution $P_{\text{CN}}(s)$ and the FN spacing distribution $P_{\text{FN}}(s)$ for interacting fermion/boson systems with and without spin degree of freedom. The system Hamiltonian is modelled by an embedded GOE of one plus two-body interactions [EGOE(1+2)]. In the past, it was shown [10] that only with proper spectral unfolding, EE exhibits GOE level fluctuations. Our numerical results for various examples of fermion/boson system and shell model, are consistent with the recently derived analytical expressions using a 3×3 random matrix model and other related quantities [30]. This establishes that these analytical expressions are universal. Also, it shows that for strong enough interaction, the local level fluctuations generated by EE follow the results of classical Gaussian ensembles.

Acknowledgements

One of the authors (NDC) thanks V K B Kota for useful discussions. PR and NDC acknowledge financial support from Science and Engineering Research Board, Department of Science and Technology (DST), Government of India (Project No.: EMR/2016/001327).

References

- [1] J Wishart, *Biometrika* **20A**, 32 (1928)
- [2] E P Wigner, *Ann. Math.* **62**, 548 (1955)
- [3] V Plerou, P Gopikrishnan, B Rosenow, L A Nunes Amaral and H E Stanley, *Phys. Rev. Lett.* **83**, 1471 (1999)
- [4] R N Mantegna and H E Stanley, *An introduction to econophysics: Correlations and complexity in finance* (Cambridge University Press, Cambridge, 1999)
- [5] J Verbaarschot, Quantum chromodynamics, in: *The Oxford handbook of random matrix theory* edited by G Akemann, J Baik and P Di Francesco (Oxford University Press, Oxford, 2011)
- [6] P Seba, *Phys. Rev. Lett.* **91**, 198104 (2003)
- [7] F Haake, *Quantum signatures of chaos*, Third edn (Springer, Heidelberg, 2010)
- [8] O Bohigas, M J Giannoni and C Schmit, *Phys. Rev. Lett.* **52**, 1 (1984)
- [9] M V Berry and M Tabor, *Proc. Roy. Soc. (London) A* **356**, 375 (1977)
- [10] T A Brody, J Flores, J B French, P A Mello, A Pandey and S S M Wong, *Rev. Mod. Phys.* **53**, 385 (1981)
- [11] A M Garcia-Garcia, T Nosaka, D Rosa and J Verbaarschot, *Phys. Rev. D* **100**, 026002 (2019)
- [12] G Akemann, M Kieburg, A Mielke and T Prosen, *Phys. Rev. Lett.* **123**, 254101 (2019)
- [13] S Jalan, *Pramana – J. Phys.* **84**, 285 (2015)
- [14] C Sarkar and S Jalan, *Chaos* **28**, 102101 (2018)
- [15] A Rai, A V Menon and S Jalan, *Sci. Rep.* **4**, 6368 (2015)
- [16] F J Dyson and M L Mehta, *J. Math. Phys.* **4**, 701 (1963)
- [17] M V Berry, *Proc. Roy. Soc. (London) A* **400**, 229 (1985)
- [18] M V Berry, *Nonlinearity* **1**, 399 (1988)
- [19] V Oganessian and D A Huse, *Phys. Rev. B* **75**, 155111 (2007)
- [20] N D Chavda and V K B Kota, *Phys. Lett. A* **377**, 3009 (2013)
- [21] N D Chavda, H N Deota and V K B Kota, *Phys. Lett. A* **378**, 3012 (2014)
- [22] N D Chavda, *Pramana – J. Phys.* **84**, 309 (2015)
- [23] L Sa, P Ribeiro and T Prosen, *Phys. Rev. X* **10**, 021019 (2020)
- [24] A L Corps and A Relano, *Phys. Rev. E* **101**, 022222 (2020)
- [25] S H Tekur, U T Bhosale and M S Santhanam, *Phys. Rev. B* **98**, 104305 (2018)
- [26] P Rao, M Vyas and N D Chavda, in *Eur. Phys. J. Spec. Top* **229**, 2603 (2020)
- [27] T A Brody, *Lett. Nuovo Cimento* **7**, 482 (1973)
- [28] K Roy, B Chakrabarti, N D Chavda, V K B Kota, M L Lekala and G J Rampho, *EPL* **118**, 46003 (2017)
- [29] A Sarkar, M Kothiyal and S Kumar, *Phys. Rev. E* **101**, 012216 (2020)
- [30] S C L Srivastava, A Lakshminarayanan, S Tomsovic and A Backer, *J. Phys. A* **52**, 025101 (2019)
- [31] A Lakshminarayanan, S C L Srivastava, R Ketzmerick, A Backer and S Tomsovic, *Phys. Rev. E* **94**, 010205(R) (2016); S Tomsovic, A Lakshminarayanan, S C L Srivastava and A Backer, *Phys. Rev. E* **98**, 032209 (2018)
- [32] V K B Kota, *Phys. Rep.* **347**, 223 (2001)
- [33] H A Weidenmüller and G E Mitchell, *Rev. Mod. Phys.* **81**, 539 (2009)
- [34] J M G Gomez, K Kar, V K B Kota, R A Molina, A Relaño and J Retamosa, *Phys. Rep.* **499**, 103 (2011)
- [35] V K B Kota and N D Chavda, *Int. J. Mod. Phys. E* **27**, 1830001 (2018)
- [36] V K B Kota, *Embedded random matrix ensembles in quantum physics* (Springer, Heidelberg, 2014)

- [37] R J Leclair, R U Haq, V K B Kota and N D Chavda, *Phys. Lett. A* **372**, 4373 (2008)
- [38] R A Davison, W Fu, A Georges, Y Gu, K Jensen and S Sachdev, *Phys. Rev. B* **95**, 155131 (2017)
- [39] K J Bulycheva, *J. High Energy Phys.* **12**, 069 (2017)
- [40] V Rosenhaus, *J. Phys. A* **52**, 323001 (2019)
- [41] V K B Kota, N D Chavda and R Sahu, *Phys. Lett. A* **359**, 381 (2006)
- [42] M Vyas, N D Chavda, V K B Kota and V Potbhare, *J. Phys. A* **45**, 265203 (2012)
- [43] H N Deota, N D Chavda, V K B Kota, V Potbhare and M Vyas, *Phys. Rev. E* **88**, 022130 (2013)
- [44] N D Chavda, V Potbhare and V K B Kota, *Phys. Lett. A* **311**, 331 (2003); *Phys. Lett. A* **336**, 47 (2004)
- [45] N D Chavda, V K B Kota and V Potbhare, *Phys. Lett. A* **376**, 2972 (2012)
- [46] M Vyas, V K B Kota and N D Chavda, *Phys. Rev. E* **81**, 036212 (2010)
- [47] N D Chavda and V K B Kota, *Ann. Phys. (Berlin)* **529**, 1600287 (2017)
- [48] T Papenbrock and H A Weidenmuller, *Rev. Mod. Phys.* **79**, 997 (2007)
- [49] V K B Kota and S Sumedha, *Phys. Rev. E* **60**, 3405 (1999)
- [50] Ph Jacquod and D L Shepelyansky, *Phys. Rev. Lett.* **79**, 1837 (1997)



Contents lists available at ScienceDirect

Materials Today: Proceedings

journal homepage: www.elsevier.com/locate/matpr

Effect of symmetry on quantum transport across disordered networks connected by many-body interactions

Priyanka Rao ^{*}, N.D. Chavda

Department of Applied Physics, Faculty of Technology and Engineering, The Maharaja Sayajirao University of Baroda, Vadodara 390001, India

ARTICLE INFO

Article history:

Received 10 September 2020

Accepted 13 October 2020

Available online xxxx

Keywords:

Quantum transport
Disordered networks
Complex systems
Many-body interactions
Embedded Ensembles

ABSTRACT

The efficient transport of particles or excitations (known as quantum efficiency) within a quantum system is a very important as well as a challenging part of nanotechnology. It plays a crucial role in devices at nano-scale, solar cell physics, quantum computers, photosynthesis, etc. Hence, it is important to find out under what conditions near-to-perfect transport between two states of such small disordered interacting quantum system can be improved. In the present work, we study influence of centrosymmetry on transport efficiencies of an initial localized excitation in disordered finite network, modeled by k -body Embedded Gaussian Orthogonal Ensembles of random matrices $EGOE(k)$. Here firstly we analyze disordered fermionic network of d sites, modeled by three different ensembles that include many-body interactions: (i) $EGOE(k)$ without centrosymmetry, (ii) $EGOE(k)$ with centrosymmetry present in both k as well as in m particle spaces [denoted as $csEGOE(k)$] and (iii) $EGOE(k)$ with centrosymmetry present in k -particle space (not in the m -particle space) [denoted as $EGOE(k-cs)$]. Similarly, we also analyze disordered bosonic network modeled by these three ensembles. We found that presence of centrosymmetry enhances quantum efficiency both for fermionic as well as bosonic networks. The results agree with those obtained in the past by Ortega et al. [Ann. Phys. (Berlin) 527 (2015) 748].

© 2020 Elsevier Ltd. All rights reserved.

Selection and peer-review under responsibility of the scientific committee of the Recent Advancements in Materials science And Nanotechnology conference.

1. Introduction

In last about half a century, the world witnessed evolutionary miniaturization of electronic devices from macro to micro scale. This in-turn, resulted in a rapidly developing field of nanoscience and nanotechnology, due to the significant properties that appear because of novel quantum effects at nano-scale. A very important as well as a challenging part of this field is Quantum efficiency, which addresses the efficient transport of particles or excitations across complex quantum systems. It plays a crucial role in designing nano-scale devices with increased efficiency [1]. Recently, in the field of condensed matter physics, quantum transport is studied in one dimensional nano wires (which may have spintronics applications), Quantum Anomalous Hall (QAH) phase with ultracold atoms, graphene and carbon nanotubes [2], quantum dots [3], solar cells [4], superconducting nanocircuits [5,6], nano-scale MOSFET devices [2,7–9]. Quantum efficiency also plays an impor-

tant role in various other fields such as, quantum information science [10–12], biomolecules [13–18], quantum optics, etc.

So far, various approaches have been developed to study quantum transport in complex quantum systems. Some of these approaches include the Landauer formula and Buttiker probes, Boltzmann transport models, scattering approach [19], non-equilibrium Green's function (NEGF) formalism, Density Functional Theory (DFT) [20], etc. The NEGF formalism being the most frequently used [1]. These systems can also be modeled by a disordered random network of nodes and links [21,22]. Random Matrix Theory (RMT) initially introduced by Wigner and Dyson in nuclear physics, is now being successfully applied to many other fields. A lot of progress has been achieved for quantum transport in open systems using scattering matrix and random-matrix theory of quantum transport. Topological superconductors, chaotic cavities [23], metallic carbon nanotubes [24], quantum dot and disordered wire ([25] and references therein) have been studied using these approaches. On the other hand, for quantum transport in closed systems, random Hamiltonian approach is used. One way is to use RMT. This is studied for disordered quantum dots [26]. However, quantum transport in closed systems remains barely studied.

^{*} Corresponding author.

E-mail address: pnrao-apphy@msubaroda.ac.in (P. Rao).

These studies suggest that RMT is well positioned to explore the universal aspects of quantum transport. However, realistic systems consist of few-body interactions among its constituents, which are not considered in classical random matrix ensembles (especially Gaussian Orthogonal Ensemble (GOE)). Embedded random-matrix ensembles of k -body interaction (in our case Embedded Gaussian Orthogonal Ensemble EGOE(k)) [27] address these few-body interactions also, that are reflected by the correlations in these networks. Using a disordered network of d sites and employing GOE for the Hamiltonian, it was shown in [28] that highly efficient quantum transport is possible for the Hamiltonian with centrosymmetry and a dominant doublet spectral structure. Recently, it has been shown by Ortega et al. that the transport efficiency can be enhanced just with centrosymmetry when GOE is replaced by EGOE(k) [29–32]. These works show that efficient quantum transport is achieved when the Hamiltonian preserves centrosymmetry.

In one dimensional nanowires, graphene, quantum dots, solar cells, nano-scale devices, etc. fermions play a very important role. Also, in QAH phase with ultracold atoms and superconducting nanocircuits bosons play an important role. This motivated us to study quantum transport across disordered (fermionic/bosonic) networks. In the present work, we study the role of centrosymmetry on transport efficiencies across disordered finite networks of m (fermions/bosons) distributed in N single particle (sp) states, connected via k -body interactions and modeled by embedded random-matrix ensembles of k -body interaction. For fermions these ensembles are symbolized as EGOE(k) and for bosons they are symbolized as BEGOE(k). We have used three different ensembles that include many-body interactions for both fermionic and bosonic networks. It is seen that presence of centrosymmetry in these networks enhances quantum efficiency. However, in the absence of centrosymmetry (or non-centrosymmetric structure of the Hamiltonian), quantum transport is not enhanced. Quantum transport across non-centrosymmetric structures is studied by various groups using various other approaches as well. Some of these include the very recent works on magnetic and electrical transport in non-centrosymmetric Nd_7Ni_2Pd [33] and charge transport in non-centrosymmetric superconductors [34].

The rest of this paper is organized as follows. Section 2 describes construction of embedded Gaussian ensembles for fermions and bosons, transport efficiency, definition of centrosymmetry and hence the construction of centrosymmetric embedded Gaussian ensembles. Section 3 presents the results and finally, we draw conclusions in Section 4.

2. Embedded ensembles for disordered networks: introducing centrosymmetry

In this paper we have modeled the fermionic and bosonic disordered networks using Embedded Gaussian Orthogonal Ensemble of k -body interaction to study the role of centrosymmetry in quantum transport across them. The nodes of the network are the basis states of the Hilbert space and the correlations among matrix elements are related to the links of the network.

2.1. Embedded ensembles

Consider a system which contains m fermions (or bosons) interacting via k -body interaction ($k \leq m$), which occupy N sp states. Let the N sp states be denoted by $|n_i\rangle$, where $i = 1, 2, \dots, N$. Initially, a k -particle Hamiltonian matrix is constructed. Employing the concepts of direct product space and Lie algebra, this k -particle Hamiltonian matrix is further embedded to the m -particle space. Here, the information in k -particle space is propagated to m -particle

space using Lie algebra. In the present study, GOE embedding is considered and these ensembles are called EGOE(k) for fermions (BEGOE(k) - for bosons). The Hamiltonian for such a system is given by,

$$H = \sum_{k_a, k_b} V_{k_a, k_b} A^\dagger(k_a) A(k_b) \quad (1)$$

Here the term V_{k_a, k_b} is the Gaussian random variate with zero mean and constant variance,

$$\overline{V_{k_a, k_b} V_{k'_a, k'_b}} = v_0^2 (1 + \delta_{k_a, k'_a} \delta_{k_b, k'_b}) \quad (2)$$

Here, the overbar denotes the ensemble average and $v_0 = 1$ without the loss of generality.

For fermions, $A^\dagger(k_a) = f_{n_1}^\dagger f_{n_2}^\dagger$ and $A(k_a) = (A^\dagger(k_a))^\dagger$ ($n_1 < n_2$). Whereas for bosons $A^\dagger(k_a) = C b_{n_1}^\dagger b_{n_2}^\dagger$ and $A(k_a) = (A^\dagger(k_a))^\dagger$ ($n_1 \leq n_2$). Here C is the normalization constant given by $C = \prod_{i=1}^2 (n_i!)^{1/2}$. Also, $f_{n_i}^\dagger$ and f_{n_i} are the fermionic creation and annihilation operators respectively and $b_{n_i}^\dagger$ and b_{n_i} are the bosonic creation and annihilation operators respectively. For fermionic network, V_{k_a, k_b} are antisymmetrized while they are symmetrized for bosonic network. The Hamiltonian H in the k -particle space has matrix dimension $d_k = \binom{N}{k}$ for fermions ($d_k = \binom{N+k-1}{k}$ for bosons). When $k = m$, EGOE(k) (or BEGOE(k)) reduces to GOE. This generates many-particle basis of dimension $d = \binom{N}{m}$ for fermions ($d = \binom{N+m-1}{m}$ for bosons). Refer [27,35–38] and references therein for further details.

2.2. Transport efficiency

In realistic complex quantum systems, only a limited degree of control is available. Hence, it is very important to find out under what conditions near-to-perfect transport between two states of a small disordered interacting quantum system can be improved [21]. Such systems can be modeled by a disordered random network of nodes and links [21,22]. Initially, the network is prepared in state $|in\rangle = |n_i\rangle$ and an excitation is introduced. Here, during the state transfer, only the state $|in\rangle$ is controlled and there is no control over its dynamics. As the network evolves unitarily, the excitation propagates to the state $|out\rangle = |n_f\rangle$. Note that the initial $|n_i\rangle$ and final $|n_f\rangle$ excitations are localized on the nodes of the network. Then, the maximum transition probability achieved among these states within a time interval $[0, T]$ is termed as the transport efficiency, which is quantitatively defined as [21,39]

$$P_{i,f} = \max_{[0, T]} |\langle n_f | U(t) | n_i \rangle|^2 \quad (3)$$

Here, $U(t)$ is the unitary quantum evolution associated with the Hamiltonian H of the network. The network is said to have perfect state transfer (PST) when $P_{i,f} = 1$ [11].

In general, random disorder adds a constraint to transport due to Anderson localization. Hence, it is necessary to identify structural elements which provide efficient quantum transport in the presence of disorder [29]. Realistic systems preserve additional symmetries (in addition to particle number m) like angular momentum, parity, spin-isospin SU(4) symmetry, and so on [27]. Various works suggest that additional strong correlations arise when realistic systems preserve centrosymmetry, which in turn remarkably enhances the state transport across such systems [28,40–42]. In addition to centrosymmetry, decoherence can also enhance efficiency in disordered networks [29]. However, there is ongoing debate on the relation between coherence and efficiency [39].

2.3. Introducing centrosymmetry in embedded ensembles

Now let us define centrosymmetry. A symmetric $d \times d$ matrix H is defined as centrosymmetric if it commutes with the exchange matrix J i.e. $JH = HJ$. The exchange matrix J is defined by $J_{ij} = \delta_{i,d-i+1}, \delta_{ij}$ is the Kronecker delta. The exchange matrix is simply an antidiagonal identity matrix [43]. In the present work, the matrix H is constructed using Embedded Gaussian Orthogonal Ensembles with and without centrosymmetry. Centrosymmetry can be introduced to the k -body embedded ensembles using the following approaches given in [30]: (i) either at the one-particle level, which is the core for the definition of the k and m particle Hilbert spaces, (ii) at the k -body level, where the actual (random) parameters of the embedded ensembles are set, or (iii) at the m -body level, which defines the dynamics.

In the present work, we study transport efficiencies in a small fermionic as well as bosonic network by employing three models: (i) EGOE(k) (and BEGOE(k)) without centrosymmetry, (ii) EGOE(k) (and BEGOE(k)) with centrosymmetry present in both k as well as m particle space [denoted by csEGOE(k) (and csBEGOE(k))] and (iii) EGOE(k) (and BEGOE(k)) with centrosymmetry present in k -particle space [denoted by EGOE(k -cs) (and BEGOE(k -cs))]. In csEGOE(k) (and csBEGOE(k)) case, centrosymmetry is imposed in the one particle space and propagated to k and m particle spaces [29–31] while in EGOE(k -cs) (and BEGOE(k -cs)), centrosymmetry is imposed in k -particle space and then propagated to m -particle space using the many-particle Hilbert space geometry. In the first case, the final Hamiltonian preserves centrosymmetric structure while it is not preserved in the latter case.

3. Results

3.1. Transport efficiency for fermions

Initially, we study the role of centrosymmetry in quantum transport across fermionic networks. We consider network gener-

ated by distributing $m = 1$ to $N-1$ fermions in $N = 6$. We vary the body rank of interaction k from 1 to m . We computed distribution of best efficiencies P for each member of the ensemble as the distribution of efficiencies of the ensemble is rather broad. We present the average value (mean) of best efficiencies P by open squares with vertical bars representing the widths of the distributions and results are shown as a function of interaction rank k . Here, it is important to consider all body rank of interactions as in bio-molecules, correlations among many particles can be present. In each calculation, an ensemble of 2000 members is used. Fig. 1 represents the probability distributions of the best efficiencies P as a function of body rank of interaction k for (i) EGOE(k) (red squares) (ii) csEGOE(k) (black squares) and (iii) EGOE(k -cs) (green squares). One can observe that the transport efficiencies for EGOE(k) (network with lack of centrosymmetry) is less than 80% for various values of m and k . However, it can be seen that below and at half-filling only for $k = m = 1$ the transport efficiency reaches above 90% while above half filling, for $m = 5$ the transport efficiencies roughly reach 80%.

Now, let us see what happens when we introduce centrosymmetry across these networks i.e. with csEGOE(k). The black open squares in Fig. 1 represent this case. Here, there is PST for $k = 1$ for all values of m , especially when the number of fermions m is odd. Also, when k or m are odd, the Hamiltonian preserves centrosymmetric structure, as a result efficiency is enhanced. For example, for $k = 3$ and $m = 5$, transport efficiency is 95%. Also, above half filling, we obtain best efficiencies. These results are in good agreement with the previous study [30]. Further, it is very important to know, how efficient the transport will be in such quantum network if centrosymmetry is imposed in k -particle space i.e. using EGOE(k -cs). The green open squares in Fig. 1 represent this case. Here also, PST is achieved for $k = 1$ for all values of m , especially when the number of fermions m is odd. Also, when k or m are odd, efficiency is enhanced. For example, for $k = 3$ and $m = 5$, transport efficiency is 90%. However, it is important to note that in this approach, the dimension of k -particle space also plays a crucial

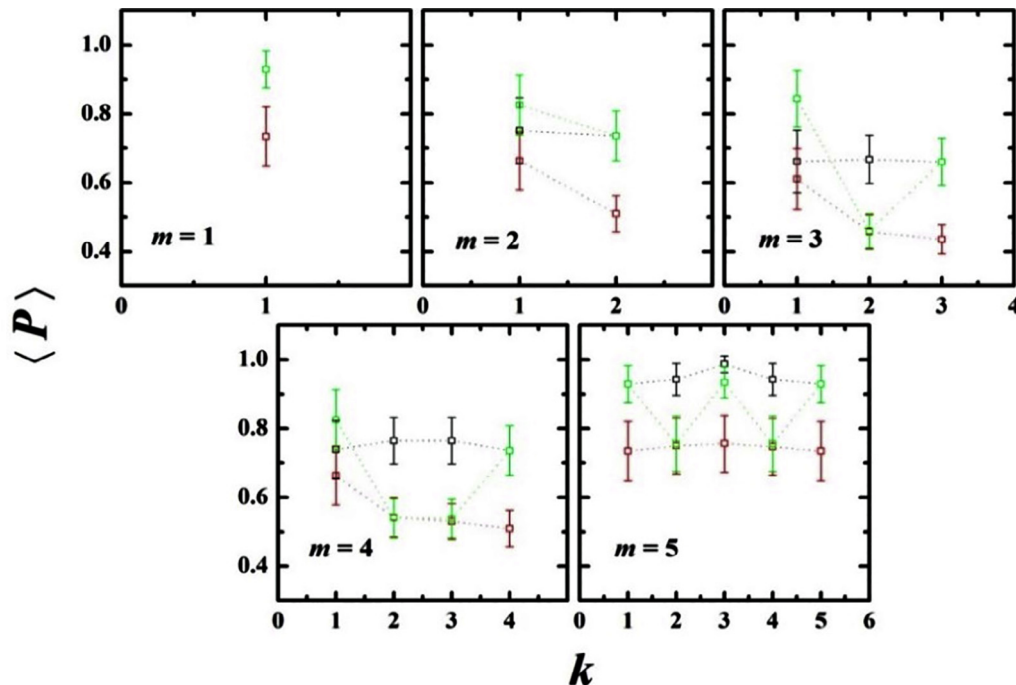


Fig. 1. Mean of the probability distributions of the best efficiencies $\langle P \rangle$ (denoted by open squares) and corresponding widths of the distributions (denoted by vertical bars) for a 2000 member (i) EGOE(k) (red squares), (ii) csEGOE(k) (black squares) and (iii) EGOE(k -cs) (green squares) as a function of body rank of interaction k . Here $N = 6$ sp states and m is varied from 1 to 5. Here dotted line is just to guide the eye. Refer text for more details. (For interpretation of the references to colour in this figure legend, the reader is referred to the web version of this article.)

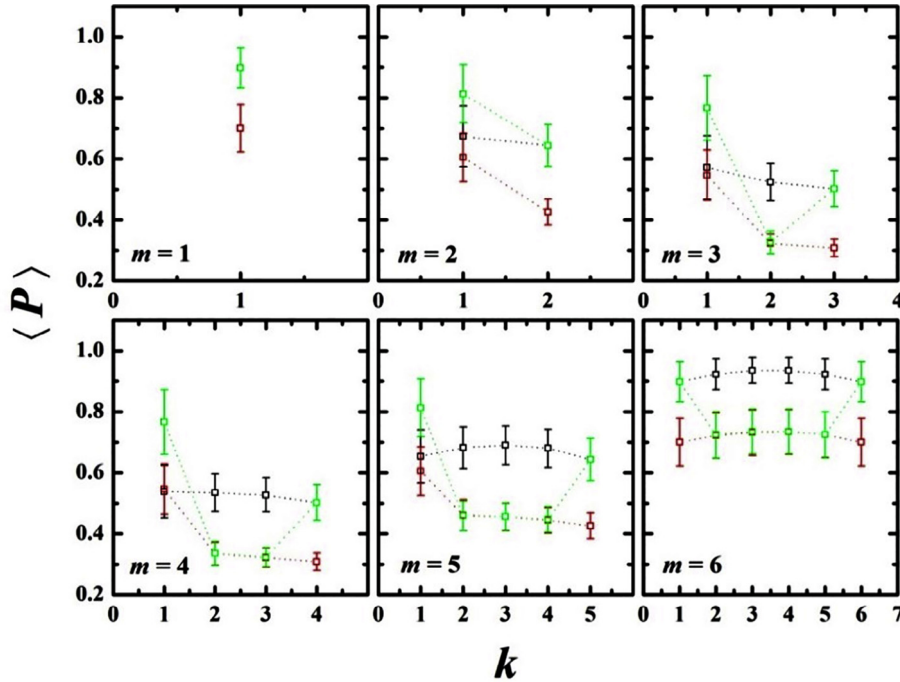


Fig. 2. Same as Fig. 1 but for network with $N = 7$ and m is varied from 1 to 6. Refer text for more details.

role. If the dimension of k -particle space is high, it decreases the transport efficiency across these networks. This suggests that even if we have odd values of k or m and above half filling, PST may not be achieved if the dimension of k -particle space is high. This proves that these studies are suitable only for phenomena and devices at nano-scale having low dimensions. We have also carried out similar analysis for $N = 7$ and the results are shown in Fig. 2. Here also we observe same trend as in the case of $N = 6$.

3.2. Transport efficiency for bosons

Now, we study the role of centrosymmetry in quantum transport across bosonic networks. It is important to note that with bosons, it is possible to have dense network, a situation not feasible for fermions due to applicability of Pauli's exclusion principle. First, we consider a network generated by basis states obtained by distributing $m = 9$ bosons in $N = 2$ sp states. The total number of basis states are $d = 10$ in this case and we represent the network Hamiltonian by a 2000 member (i) BEGOE(k), (ii) csBEGOE(k) and (iii) BEGOE(k -cs). Open squares represent the average value of probability distributions of the best efficiencies P of each member of ensemble, calculated as a function of interaction rank k . The vertical bars represent the width of probability distributions of the best efficiencies P about the mean of each member of ensemble. The results are presented in Fig. 3. The red open squares correspond to BEGOE(k) while the results for csBEGOE(k) are represented by black open squares. For a two-level ($N = 2$), csBEGOE(k) and BEGOE(k -cs) are identical by construction [30]. It is evident from the results shown in Fig. 3 that the presence of centrosymmetry enhances transport efficiencies and these results are in good agreement with those obtained in [30].

Moving further, we consider a network generated by basis states obtained by distributing $m = 6$ bosons in $N = 3$ sp states. The dimensionality of the network is $d = 28$ in this case. Here, we varied the number of bosons m from 1 to 6. The results are shown in Fig. 4. It can be seen that the transport efficiency for BEGOE(k) (in absence of centrosymmetry) is less than 80% for almost all

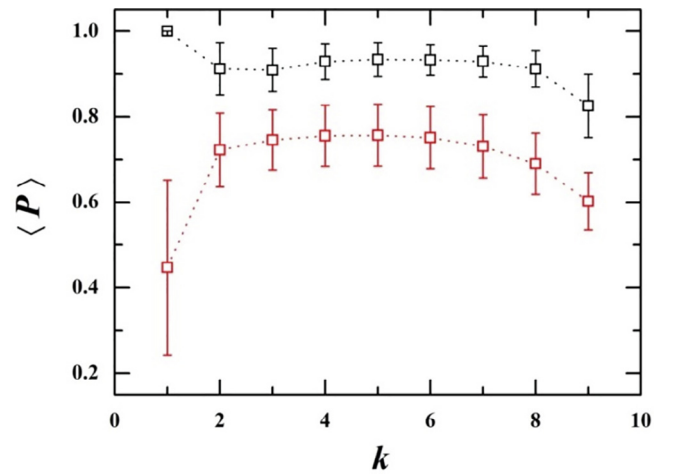


Fig 3. Mean of the probability distributions of the best efficiencies (P) (denoted by open squares) and corresponding widths of the distributions (denoted by vertical bars) for a 2000 member (i) BEGOE(k) (red squares) and (ii) csBEGOE(k) (black squares) with $N = 2$ sp states and $m = 9$ as a function of body rank of interaction k . Here dotted line is just to guide the eye. Note that, BEGOE(k -cs) and csBEGOE(k) are identical for $N = 2$. Similar results are reported in [30]. Refer text for more details. (For interpretation of the references to colour in this figure legend, the reader is referred to the web version of this article.)

the cases. With BEGOE(k -cs), there is a marginal improvement for all $k > 1$ as centrosymmetry structure is lost in m -particle space although it is present in k -particle space. While on the other hand, in presence of centrosymmetry, with csBEGOE(k), one can observe that the efficiency is around 90% for $k \leq 3$. This clearly demonstrates that the presence of centrosymmetry enhances the transport efficiency. Note that for $k=m$, BEGOE(k -cs) and csBEGOE(k) are identical and they are GOE with centrosymmetry. For csBEGOE(k), there is a PST for $m = 3$ and $k \leq 3$. It is interesting to note that for $k = m = 1$, BEGOE(k -cs) gives PST for $m = 1-6$. The lack of PST for $N = 3$ levels beyond $m = 3$ and $k \leq 3$ in comparison to

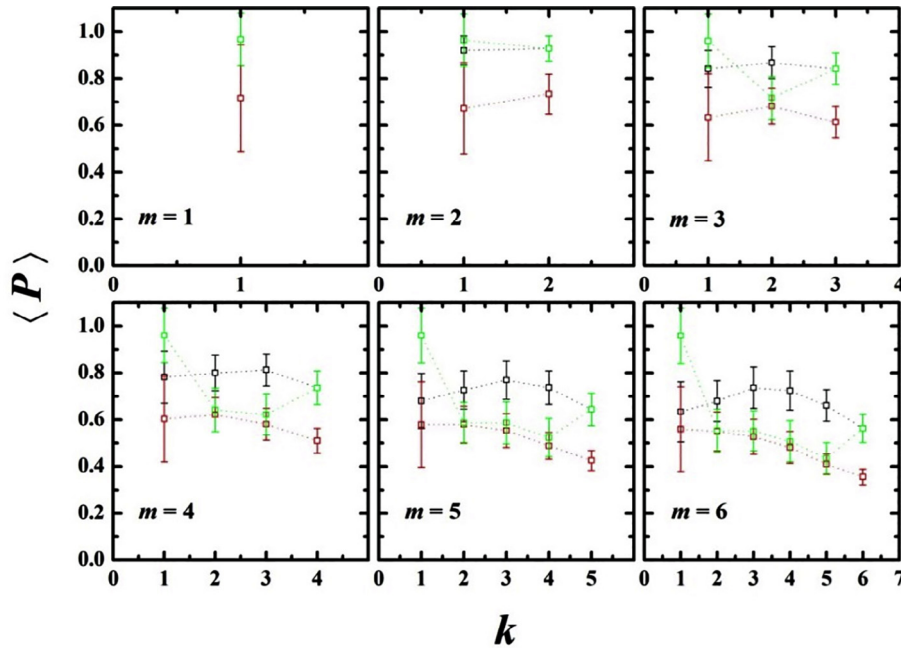


Fig 4. Same as Fig. 3 but for a 2000 member (i) BEGOE(k) (red squares), (ii) csBEGOE(k) (black squares) and (iii) BEGOE(k -cs) (green squares) as a function of body rank of interaction k . Here $N = 3$ sp states and m is varied from 1 to 6. Note that for $k = m$, results for BEGOE(k -cs) and csBEGOE(k) are identical. Refer text for more details. (For interpretation of the references to colour in this figure legend, the reader is referred to the web version of this article.)

$N = 2$ example can be attributed to a systematic appearance of doublets in the spectrum for $N = 2$ [11]. These results show the importance of presence of centrosymmetry in optimal transport across disordered (fermionic/bosonic) networks. The absence of which will lead to inefficient quantum transport.

4. Conclusions

In this paper, we have studied the effect of centrosymmetry on transport efficiency across disordered fermionic and bosonic networks modeled by k -body embedded Gaussian ensembles EGOE (k) (for fermions) and BEGOE(k) (for bosons) respectively. We found that the presence of centrosymmetry in m -particle space is responsible for the enhancement of transport efficiency in a small network and results are in good agreement with [30]. Further, we also verified that the centrosymmetry structure is essentially needed in both, k -particle as well as in m -particle space, to enhance quantum efficiency. Following the results of present work, it is possible to design networks with good efficiency even in presence of certain many-body random perturbations. For example, the efficiency in nano-structure such as quantum wires, it is interesting to check the case with filling factors close to one, where many-body interactions lead to very good efficiencies. Another example is of efficient single electron transport in a linear array of tunnel-coupled quantum dots, which can further be used as an ideal quantum channel in quantum computers [44] and efficient transmission of qubits between the different quantum registers in a quantum bus based on semiconductor self-assembled quantum dots [45]. Also, controlling strong interactions between ultracold atoms trapped in optical lattices can serve in efficient quantum computation [46]. Finally, the results in our paper can be useful to understand the good efficiency properties experimentally observed in exciton transport in certain biomolecules such as the Fenna-Matthews-Olson complex [18]. It will be interesting to study the transfer of quantum states from one location to another which is the base of Quantum Information Science, using Embedded Ensembles with spin degree of freedom.

Credit author statement

All authors contributed equally and agreed to the published version of the manuscript.

Declaration of Competing Interest

The authors declare that they have no known competing financial interests or personal relationships that could have appeared to influence the work reported in this paper.

Acknowledgements

Authors thank V. K. B. Kota and Manan Vyas for many useful discussions. Authors acknowledge support from Department of Science and Technology (DST), Government of India [Project No.: EMR/2016/001327].

References

- [1] S. Datta, *Quantum Transport: Atom to Transistor*, Cambridge University Press, New York, 2015.
- [2] M. W. Chuan, et.al *Superlattices and Microstructures* 140 (2020) 106429/1-106429/17.
- [3] S. Kumar, *J. Phys.: Condens. Matter* 31 (2019) 200301.
- [4] J. Nelson, *The Physics of Solar Cells*, Imperial College Press, London, 2010.
- [5] A. Romito, R. Fazio, C. Bruder, *Phys. Rev. B* 71 (2005) 100501/1-100501/4.
- [6] M. Paternostro, G. M. Palma, M. S. Kim, G. Falci, *Phys. Rev. A* 71 (2005) 042311/1-042311/6.
- [7] A. Svizhenko, P. Anantram, T.R. Govindan, B. Biegel, R. Venugopal, *J. Appl. Phys.* 91 (2002) 2343–2354.
- [8] Z. Ren, R. Venugopal, S. Goasguen, S. Datta, M. Lundstrom, *IEEE Trans. Electron Devices* 50 (2003) 1914–1925.
- [9] X. Shao, Z. Yu, *Solid-State Electronics* 49 (2005) 1435–1445.
- [10] M. Christandl, N. Datta, A. Ekert, A.J. Landahl, *Phys. Rev. Lett.* 92 (2004) 187902/1-187902/4.
- [11] M. Christandl, N. Datta, T. C. Dorlas, A. Ekert, A. Kay, A. J. Landahl, *Phys. Rev. A* 71 (2005) 032312/1-032312/11.
- [12] N. Gisin, G. Ribordy, W. Tittel, H. Zbinden, *Rev. Mod. Phys.* 74 (2002) 145–195.
- [13] T. Scholak, F. de Melo, T. Wellens, F. Mintert, A. Buchleitner, *Phys. Rev. E* 83 (2011) 021912/1-021912/4.
- [14] X. Hu, K. Schulten, *Phys. Today* 50 (1997) 28–34.
- [15] H. Lee, Y.-C. Cheng, G.R. Fleming, *Science* 316 (2007) 1462–1465.

- [16] G.D. Scholes, T. Mirkovic, D.B. Turner, F. Fassioli, A. Buchleitner, *Energy Environ. Sci.* 5 (2012) 9374–9393.
- [17] G.D. Scholes et al., *Nature (London)* 543 (2017) 647.
- [18] R.E. Fenna, B.W. Matthews, *Nature (London)* 258 (1975) 573–577.
- [19] Y.V. Nazarov, Y.M. Blanter, *Quantum Transport: Introduction to Nanoscience*, Cambridge University Press, New York, 2009.
- [20] H. Sadeghi, *Nanotechnology* 29 (2018) 373001.
- [21] M. Walschaers, J. F. d. C. Diaz, R. Mulet, A. Buchleitner, *Phys. Rev. Lett.* 111 (2013) 180601/1–180601/5.
- [22] J. Adolphs, T. Renger, *Biophys. J.* 91 (2006) 2778–2797.
- [23] A. Jarosz, P. Vidal, E. Kanzielper, *Phys. Rev. B* 91 (2015) 180203/1–180203/5.
- [24] Y. Takane, K. Wakabayashi, *J. Phys. Soc. Jpn.* 72 (2003) 2710–2713.
- [25] C.W.J. Beenakker, *Rev. Mod. Phys.* 69 (1997) 731–808.
- [26] C. W. J. Beenakker, M. Buttiker, *Phys. Rev. B* 46 (1997) 1889.
- [27] V.K.B. Kota, *Embedded Random Matrix Ensembles in Quantum Physics*, Springer, Heidelberg, 2014.
- [28] M. Walschaers, J. Diaz, R. Mulet, A. Buchleitner, *Phys. Rev. Lett.* 111 (2013) 180601/1–180601/5.
- [29] A. Ortega, T. Stegmann, L. Benet, *Phys. Rev. E* 98 (2018) 012141/1–012141/7.
- [30] A. Ortega, M. Vyas, L. Benet, *Ann. Phys. (Berlin)* 527 (2015) 748–756.
- [31] A. Ortega, T. Stegmann, L. Benet, *Phys. Rev. E* 94 (2016) 042102/1–042102/12.
- [32] V. K. B. Kota, N. D. Chavda, *Int. J. Mod. Phys. E* 27 (2018) 1830001/1–1830001/51.
- [33] A. K. Pathak, et al. *AIP Adv.* 10 (2020) 015103/1–015103/5.
- [34] Y.M. Itahashi et al., *Sci. Adv.* 6 (2020) 1–6.
- [35] L. Benet, T. Rupp, H.A. Weidenmuller, *Ann. Phys. (N.Y.)* 292 (2001) 67–94.
- [36] M. Vyas, Ph.D. Thesis, (M.S. University of Baroda, Vadodara, India, 2011), arXiv:1710.0833 (2017).
- [37] V.K.B. Kota, N.D. Chavda, *Entropy* 20 (2018) 541/1–541/22.
- [38] M. Vyas, T.H. Seligman, *AIP Conf. Proc.* 1950 (2018) 030009.
- [39] T. Zech, R. Mulet, T. Wellens, A. Buchleitner, *New J. Phys.* 16 (2014) 055002/1–055002/16.
- [40] M. Walschaers, R. Mulet, T. Wellens, A. Buchleitner, *Phys. Rev. E* 91 (2015) 042137/1–042137/15.
- [41] M. Walschaers, A. Buchleitner, M. Fannes, *New J. Phys.* 19 (2017) 023025/1–023025/19.
- [42] M. Walschaers, R. Mulet, A. Buchleitner, *J. Phys. B* 50 (2017) 224003.
- [43] A. Cantoni, P. Butler, *Linear Algebra Appl.* 13 (1976) 275–288.
- [44] G.M. Nikolopoulos, D. Petrosyan, P. Lambropoulos, *Europhys. Lett.* 65 (2004) 297–303.
- [45] I. D'Amico, *Microelectronics J.* 37 (2006) 1440–1441.
- [46] L.M. Duan, E. Demler, M.D. Lukin, *Phys. Rev. Lett.* 91 (2003) 090402.